Changes in precipitation and temperature patterns related to the state of the North Atlantic Ocean during the Medieval Climate Anomaly

Shailendra Pratap[1], Yannis Markonis[1], and Cécile L. Blanchet[2]

[1]Faculty of Environmental Sciences, Czech University of Life Sciences Prague, Kamýcká 129, Praha– Suchdol, 165 00, Czech Republic
[2]Section Geomorphology, Helmholtz Centre Potsdam, GFZ German Research Centre for Geosciences, Potsdam, Germany

Correspondence: Shailendra Pratap (pratap@fzp.czu.cz)

Abstract.

In a warmer climate, uncertainties persist regarding regional precipitation responses and a potential weakening of the Atlantic Meridional Overturning Circulation (AMOC). This study examines the Medieval Climate Anomaly (~800–1399 CE) warm period to uncover hydroclimate patterns and their links with the North Atlantic Ocean variability, including AMOC, Sea Surface Temperature (SST), and the Inter-Tropical Convergence Zone (ITCZ) at centennial (100-years) scales. Analyzing change-sensitive multi-proxy data reveals that North Atlantic Ocean conditions play a significant role in influencing hydroclimate variability across Europe and North America, potentially by regulating atmospheric heat and moisture transport. Specifically, we show that warm SST conditions correspond to warmer climates on both continents, while low SST periods are associated with a southward shift of the ITCZ, potentially initiating cooler climates and hydrological variations. However, the state of the AMOC remains unclear, despite indications of subtle weakening in some records. Exploring hydroclimate suggests that continental-scale precipitation variations are linked to temperature changes, but regional responses are uncertain. Notably, warmer/slightly warmer climates are primarily linked to more humid conditions, especially in mid-latitude regions. Conversely, slightly colder climates tend to result in more arid conditions. Comparing model assimilation with proxy data reveals significant discrepancies, suggesting that either the models fail to adequately capture key processes or the proxy data contain substantial uncertainties. While our findings provide valuable insights into regional hydroclimate changes and variability in the North Atlantic Ocean state under a warmer climate, they also emphasize the necessity for more in-depth research on regional precipitation variability and the identification of appropriate proxies for tracking AMOC signals.

1 Introduction

A warmer climate will have far-reaching impacts on socioeconomic life by altering the hydrological cycle and affecting water resources. In recent few decades, significant changes have occurred in the global hydrological cycle (Hobeichi et al., 2022), and it is expected that future global warming will cause even more alterations in precipitation patterns (Thackeray et al., 2022). Most studies project an intensification of the hydrological cycle in warmer climates (Trenberth et al., 2003; Douville et al.,

2021). This is because warm conditions increase the atmospheric moisture holding limit, which will lead to more intense precipitation (Held and Soden, 2006). However, some studies have also documented drier conditions in a warmer climate

25 (Dai, 2013; Huang et al., 2016). Owing to these conflicting findings, the behavior of the hydrological cycle in a warm climate remains enigmatic, although there is substantial evidence of its intensification as temperature increases in the paleoclimatic records (Pratap and Markonis, 2022; Konecky et al., 2023).

In addition to directly modulating the hydrological cycle, warmer conditions also exert strong indirect controls over oceanic states. Specifically, a warmer climate influences glaciers and Sea Surface Temperature (SST), leading to the melting of ice

30 sheets and sea ice, respectively. This melting subsequently affects global ocean circulation patterns, thereby impacting hydro-climate variables such as temperature and precipitation patterns (Zhuravleva et al., 2023). The discharge of freshwater into the North Atlantic Ocean from melting ice masses is known to disturb ocean circulation patterns (Kuhlbrodt et al., 2007), leading to cascading impacts on both regional and global hydroclimate systems. In a warmer climate, the changes observed in SST and the Atlantic Meridional Overturning Circulation (AMOC) compared to the preceding decades have drawn significant

35 global attention. The thermohaline circulation, i.e., the AMOC is a chain of ocean currents system that carries warm and salty surface-waters northwards (from the Equatorial regions towards the Arctic). These surface waters subsequently sink down and lose buoyancy over the Arctic region and move southwards (from the Arctic towards Equatorial regions) as cold deep-waters. During this circulation process, the AMOC redistributes atmospheric heat and moisture, which exerts a strong control on the global water cycle (Marshall et al., 2014; Latif et al., 2022) and influencing hydroclimate distribution. Recently, the state of the

40 AMOC has drawn wide attention because research indicates that it is slowing down, and numerical models project a further weakening by 2100 (Boers, 2021; Masson-Delmotte et al., 2021).

There is an ongoing debate on the prevailing hypothesis that increasing global warming will weaken the AMOC (Weijer et al., 2020; Boers, 2021). Due to the increasing rate of greenhouse gases and the accompanying warm climate (Latif et al., 2022), freshwater discharge into the ocean alters the density of the surface water, making it more buoyant and less likely to

45 sink. Consequently, a decrease in the North Atlantic surface water density will likely inhibit the ocean deep-water convection and will cause a weakening of the AMOC (Böning et al., 2016). Rahmstorf (1999) and Caesar et al. (2018) suggested that the AMOC is presently in its weakest state during the past millennium, due to increasing anthropogenic global warming (Bakker et al., 2016). While a shutdown of AMOC has been projected before the end of the present century (Boers, 2021), the possibility remains uncertain and still largely debated (Kriegler et al., 2009).

50 Importantly, the variability of the AMOC has a significant impact on hydroclimates in North American and European regions (Jackson et al., 2015). The anticipated weakening of the AMOC is likely to result in reduced atmospheric moisture transport towards Europe and North America, leading to limited precipitation and cold conditions in these regions (Liu et al., 2020; Vellinga and Wood, 2002). Moreover, a slowdown of the AMOC could impact the monsoon system over Asia and Africa (Gupta et al., 2003), as well as alter moisture flows and air temperatures globally by pushing away Inter-Tropical Convergence Zone

55 (ITCZ) southward (Couchoud et al., 2009; Brovkin et al., 2021). A significant weakening of the AMOC and the consequent southward displacement of the ITCZ would likely lead to global hydroclimatic alterations, such as shifts in hydrological cycle patterns across the terrestrial regions (Liu et al., 2020).

The evidence from the distant past reveals that most of the abrupt events were in response to the Atlantic long-term variability, particularly the AMOC in specific (Weijer et al., 2019). For instance, the events such as Dansgaard-Oeschger (Santos et al.,

60   2020), the last ice age, and the deglaciation period were all responses to alterations in the AMOC (Lynch-Stieglitz, 2017). A weakened AMOC has been hypothesized in the Heinrich events (Allen et al., 1999), the Younger Dryas (Clark et al., 2012), the 8.2 ka events (Ellison et al., 2006), and particularly cold climatic phases (Aguiar et al., 2021). The majority of studies conducted thus far have focused on cooler time intervals. Interestingly, AMOC shifts often occurred during the transition time between glacial-interglacial (Bellomo et al., 2021) or interglacial-glacial periods.

65   It is still being investigated whether the current warmer climate will lead to colder climates in the future, and what relationship exists between warmer climates and AMOC variability. Therefore, understanding the relationship between AMOC variability and hydrological cycle variability, including SST and ITCZ response, in warm climates could help predict current and future hydroclimate shifts. Since SST exert a substantial influence on the distribution of hydroclimate patterns across the North Atlantic regions, a comprehensive examination of SST patterns in conjunction with hydroclimate patterns may yield

70   valuable insights into its significance (Sutton and Hodson, 2005).

However, only a few observational studies have focused on the behavior of AMOC, SST, and ITCZ, including their relationships with hydroclimate patterns during past warm climates, mainly the Medieval Climate Anomaly (MCA) period. The lack of data on past AMOC variability poses a challenge for examining AMOC variations and their possible influences on hydroclimate conditions. Additionally, climate models do not fully capture past climatic conditions and ocean circulation, which

75   hinders their ability to provide reliable conclusions and projections (Srokosz and Bryden, 2015). Consequently, AMOC variability during the MCA is still not well understood. Nevertheless, investigating the relationship between past warm climates, AMOC, and SST could be a foundation for understanding how these parameters will influence the global hydroclimate in a warm climate. Therefore, our study stands as unique due to our focus on investigating North Atlantic variability (including SST, AMOC, and ITCZ shift) and its correlation with terrestrial hydroclimate patterns during the MCA period, which was a

80   more or less warm period like the ongoing interglacial time.

Since the core period of the MCA falls within 1000 and 1300 CE, we selected a time scale from 800 to 1399 CE. This broader temporal scope enables us to examine variations occurring not only during the MCA but also in the periods preceding and succeeding this distinct climatic phase. The climate during the MCA is often suggested to have predominantly warm and arid conditions, specifically during the core period, and cold and humid conditions afterward (LaMarche Jr, 1974; Graham

85   et al., 2011). Despite the widespread acceptance of these hydroclimatic changes, the factor responsible for the abrupt decline in average temperature during the MCA-Little Ice Age (LIA) transition remains elusive. However, it has been suggested that shifting global atmospheric circulation patterns between the MCA and LIA were the main drivers of hydroclimatic changes (Lamb, 1969; Gonzalez-Rouco et al., 2011), which still needs to be tested. Our study aims to investigate changes in precipitation, mainly precipitation minus evaporation (P-E), and temperature patterns in response to centennial-scale variations in the

90   state of the North Atlantic, using regional multi-proxies.

2 Data and Methods

2.1 Data

For this study, we used a variety of proxy reconstructions available in open-source databases, specifically the NOAA's National Centers for Environmental Information (https://www.ncei.noaa.gov/access/paleo-search/) and the Past Global Changes (PAGES; https://pastglobalchanges.org/science/data/databases). We chose precipitation and temperature-sensitive material, including stalagmites, lake sediments, tree rings, ice cores, marine sediments, and peatland sediments, which are distributed across North America and Europe. These materials serve as indirect indicators of changes in P-E patterns over the locations where the materials are collected. So when we refer to precipitation, it is actually denoting P-E state. Additional information about the selected material and proxies with their specific locations can be found in Figure 1. To ensure consistent and accurate representation of the relevant variables, such as temperature and precipitation (i.e., P-E), we maintained alignment with the specific variables as indicated by the original investigators in their respective data sources. Further elaboration and details on datasets can be found in the corresponding sections, namely Table A1, Table A2, Table A3, and Table A4.

For choosing AMOC-sensitive proxies, we selected a domain over the North Atlantic regions, defined by latitude -12.9 to 87°E and longitude 5 to -90°N. Since direct measurements of AMOC started in 2004 (McCarthy et al., 2015), and instrumental data are not available for the period we investigated, we utilized well established AMOC-sensitive tracers. These included deep-sea proxies such as δ^{13}C, cadmium/calcium (Cd/Ca) ratios, and sortable silts (mean size). We have chosen to focus on these tracers for a specific reason– they serve as paleomicronutrient indicators, crucial for identifying patterns related to the migration and dynamics of deep-water masses, as these nutrients are transported via oceanic circulation (Marchitto Jr et al., 2002). Changes in the concentration of these nutrients serve as markers of the state of oceanic circulation. Monitoring these tracer concentrations in deep seawater is essential for understanding the dynamics of ocean circulation and for assessing the stability of the global ocean circulation system over time. Notably, the observed reduction in δ^{13}C values and Cd/Ca ratio within deep/intermediate seawater serves as a significant indicator of the decreased presence of North Atlantic Deep Water (Bell et al., 2014; Valley et al., 2022). Furthermore, sortable silts (10-63μm) are associated with the physical strength of deepwater flow, as they are transported by ocean currents/water masses and changes over time. Consequently, these sortable silts are valuable for providing an overview of deep ocean currents and serve as a valuable proxy for the strength of the AMOC (Hoffmann et al., 2019).

In addition, we also examined the SST and ITCZ variations to determine if they provide signals of the AMOC variation. To track the ITCZ, we reconstructed the ITCZ shift index using the δ^{18}O values recorded from stalagmite by various investigators. For this reconstruction, we used 11 δ^{18}O records from different sites located in the Northern Hemisphere (NH) and 5 δ^{18}O records from various sites in the Southern Hemisphere (SH) due to data availability limitations. All selected sites are currently positioned within the present migration path of the ITCZ across both the NH and SH. After collecting these records, the mean δ^{18}O value was calculated separately for the NH and SH. Then, the SH mean was subtracted from the NH mean to obtain the ITCZ shift index. For comparison, the ITCZ shift index reconstructions by Tan et al. (2019) and Chawchai et al. (2021) were also utilized. Changes in SST may be linked to variability in sea-ice cover, the reorganization of ocean surface currents,

125 freshwater input by melting of ice-sheets and intricate feedback processes between the atmosphere, land, and ocean. Moreover, the findings regarding ITCZ and SST variability will serve as a crucial references for anticipating future changes in the North Atlantic and their correlated impacts on the hydroclimate. In tracking SST conditions, magnesium-calcium (Mg/Ca) ratios and $U^{k'}37$ proxies are widely recognized for their effectiveness (Bendle and Rosell-Melé, 2004; Wei et al., 2000). Hence, we have incorporated these proxies into our study to assess variations in SST. Additionally, data assimilation based reconstruction

130 on ITCZ and SST from Steiger et al. (2018) have been included to assess the reliability of model-based paleoclimate outputs.

For the comparative analysis between proxies and models, assimilation data related to paleoclimate were acquired from two sources: the Paleo Hydrodynamics Data Assimilation product (PHYDA; for temperature, SST, ITCZ, and Palmer Drought Severity Index (PDSI) as an indicator of humid and arid conditions) (Steiger et al., 2018) and PaleoView (for temperature and precipitation) (Fordham et al., 2017). The PDSI is widely used to determine soil moisture availability, with higher values sug-

135 gesting increased precipitation/wet conditions, whereas lower PDSI values denote low precipitation/dry conditions. Therefore, in this study, the PDSI is utilized as an indicator of humid and arid conditions. PHYDA is a global hydroclimate reconstruction generated by combining about 2978 proxy time series with the physical constraints of atmosphere-ocean climate models. The PHYDA provides data from 1 to 2000 CE with annual means (April to March), the boreal growing season of June, July, and August (JJA), and the austral growing season of December, January, and February (DJF). In contrast, PaleoView uses

140 the TRaCE21ka experiment based on the daily simulated outcomes of the Community Climate System Model ver.3 (CCM3) (Collins et al., 2006). It provides monthly and annual scale temperature and precipitation data from 22 ka BP to 1989 CE. We gained the climate model data at the annual scale, covering the time scale of 800-1399 CE, for the specified variables.
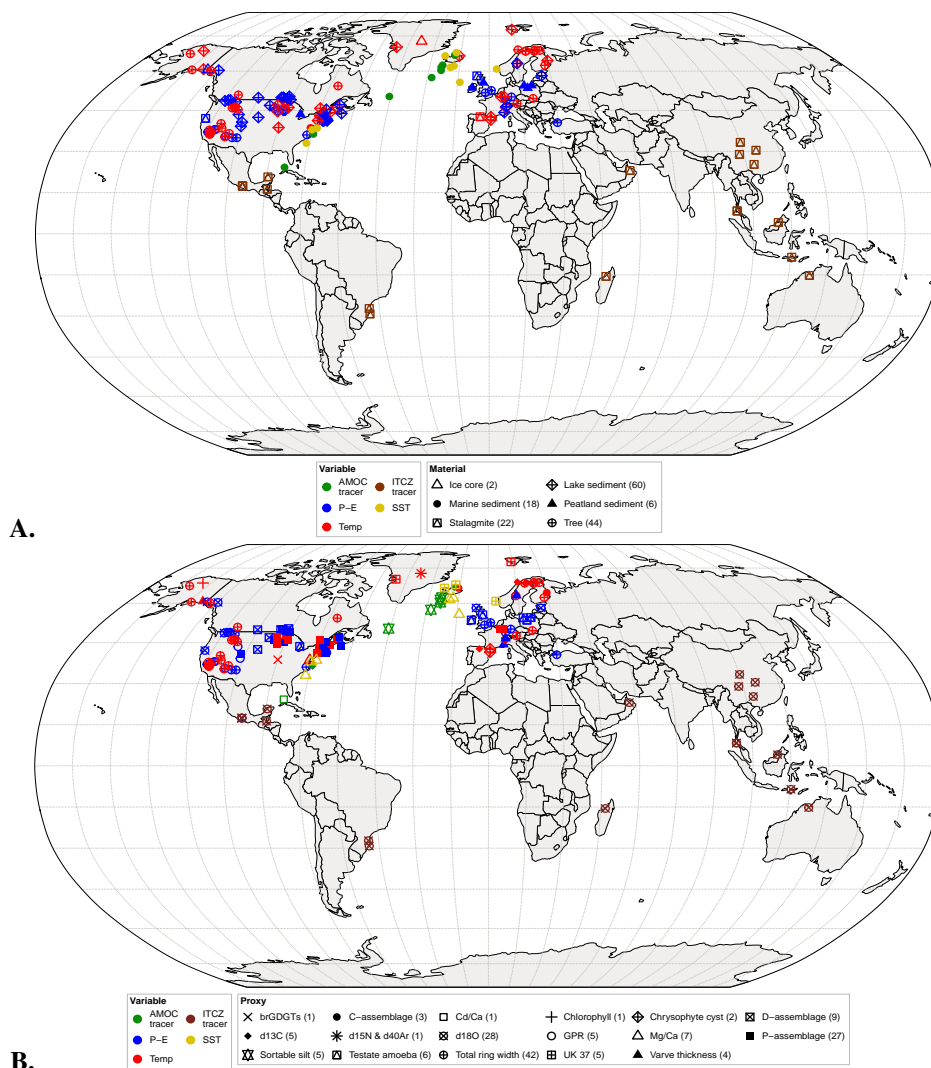
Figure 1. The map provided in this figure displays the spatial distribution of data sources categorized as material sources ('A') and proxy sources ('B'). These sources were utilized in our study to collect information related to precipitation minus evaporation (P-E), temperature (Temp), sea surface temperature (SST), Atlantic Meridional Overturning Circulation (AMOC), and the records of the Inter-Tropical Convergence Zone (ITCZ). In plot B, 'D-assemblage' denotes diatom assemblage data, 'P-assemblage' represents pollen data, and 'C-assemblage' corresponds to chironomid data. The numbers in the parentheses indicate the quantity of proxies.

2.2 Methods

After the data mining, we implemented measures to ensure the datasets were consistent. In our study, we utilized diverse
145 datasets, each with distinct units of measurement. To establish consistency and express all the data on a uniform scale, we applied a natural log transformation. Furthermore, we identified negative values in datasets, and to address this, we converted

all values to positive using Equation 1 and subsequently performed a log transformation on them.

$$y(x) = X + |\min(x)| + 1 \tag{1}$$

In Equation 1, $y(x)$ denotes the transformation that is employed to ensure that the data possesses positive values suitable for a log transformation. $|\min(x)|$ represents the minimum value within the dataset, as an absolute value. Finally, X represents the values within the data that are being converted into positive values through this transformation.

The values of $\delta^{18}O$ allow us to assess past hydrological conditions, distinguishing between humid and arid periods and reflecting the prevailing precipitation conditions. Therefore, we ensured that the $\delta^{18}O$ records were accurately represented in our analysis. Several studies have suggested a negative correlation between isotopic values (from $\delta^{13}C$ and $\delta^{18}O$) and precipitation conditions (Hong et al., 2001; Tan et al., 2019), indicating that low isotopic values correspond to increased precipitation conditions and vice versa. To align the values with this relationship, we applied a negative log transformation to reverse the $\delta^{13}C$ and $\delta^{18}O$ records, ensuring that low isotopic values correspond to low precipitation and high isotopic values correspond to high precipitation. After ensuring the correct transformation of values in all records, we standardized them by converting them into z-scores. Subsequently, these standardized values were aggregated into centennial time steps for each dataset individually. We then employed these standardized deviation values to estimate variability on a continental scale.

Finally, we performed a spatiotemporal investigation of precipitation and temperature, conducting time-series analysis (including model assimilated records, AMOC, SST, and ITCZ) to assess overall continental scale variability. To this end, we employed maps of Europe and North America to visually illustrate the regional distribution of variables, facilitating our understanding of their relationships and interconnections. The spatiotemporal representation of data proved invaluable for examining latitudinal and spatial shifts in hydroclimate regimes. All analyses were conducted using the R statistical software (R Core Team et al., 2022).

3 Results

3.1 Variability in AMOC, SST, and ITCZ during the MCA warm period

Our analysis of AMOC-sensitive tracers, at the centennial scale, indicates notably weak and/or non-significant changes in AMOC strength (Moffa-Sánchez et al., 2019). We employed multiple records to track AMOC variations, each presenting distinct signals of AMOC changes over time. The potential weakening of AMOC due to warmer climates remains uncertain (Kilbourne et al., 2022), given the divergence in responses observed across various records. It is possible that either the changes are very low or very short, or the proxies are not sensitive enough to capture AMOC weakening responses. In our dataset, specifically, both $\delta^{13}C$ and Cd/Ca exhibit weak signals of AMOC after the mid-10th century (Figure 2-A and B). Among the sortable silt records (Figure 2 C), three (NEAP-4k, Orphan Knoll, GS06-14408GC) indicate weak signals of AMOC from the 10th to 11th century, while two (MD99-2251 and ODP983) present a contrasting response during this period. We observed that sortable silt records from MD99-2251 and ODP983 revealed an early indication of a weak AMOC signal compared to $\delta^{13}C$

and Cd/Ca. Specifically, this signal emerges from the 9th century and extends from the mid-9th century to approximately the mid-10th century, respectively.

180   We observed that SST (Figure 3-A) over the North Atlantic region was high from the 9th to the mid-10th centuries. However, thereafter, SST started to decline, and between the mid-10th and 14th centuries, the average SST remained low. Notably, the SST conditions remained relatively stable and consistent with the centennial mean from the late 12th to mid-13th century. Subsequently, from the mid-13th century onward, there was a noticeable weakening observed in SST conditions. Furthermore, the confidence interval (CI) and kernel density (KD) estimation suggest statistically significant variation in SST between the

185   9th to 14th centuries (Figure 3-A). Upon analyzing the significance of SST records using the CI, it becomes evident that except for the 10th and 11th century, there is high uncertainty in the SST variability during the 9th and from the 12th to 14th centuries. Additionally, the KD estimates for the records from the 9th and 10th centuries indicate that the SST condition was higher than their centennial mean, as indicated by the Mg/Ca, $U^{k'}37$, and PHYDA records. However, a few Mg/Ca and $U^{k'}37$ records show a below-average response. Later, during the 11th to 14th century, the lowered values of Mg/Ca, $U^{k'}37$, and PHYDA

190   indicate low SST conditions, while a few Mg/Ca, $U^{k'}37$ records suggest the opposite.

In the case of the ITCZ, we observed that its variability was synchronous with fluctuations in SST. Our findings indicate that southward/northward shifts in the ITCZ are significantly associated with weak/strong phases of the AMOC. Notably, while the PHYDA ITCZ assimilation exhibits fluctuations similar to those of the proxy data, it demonstrates greater variability than the proxy observations.
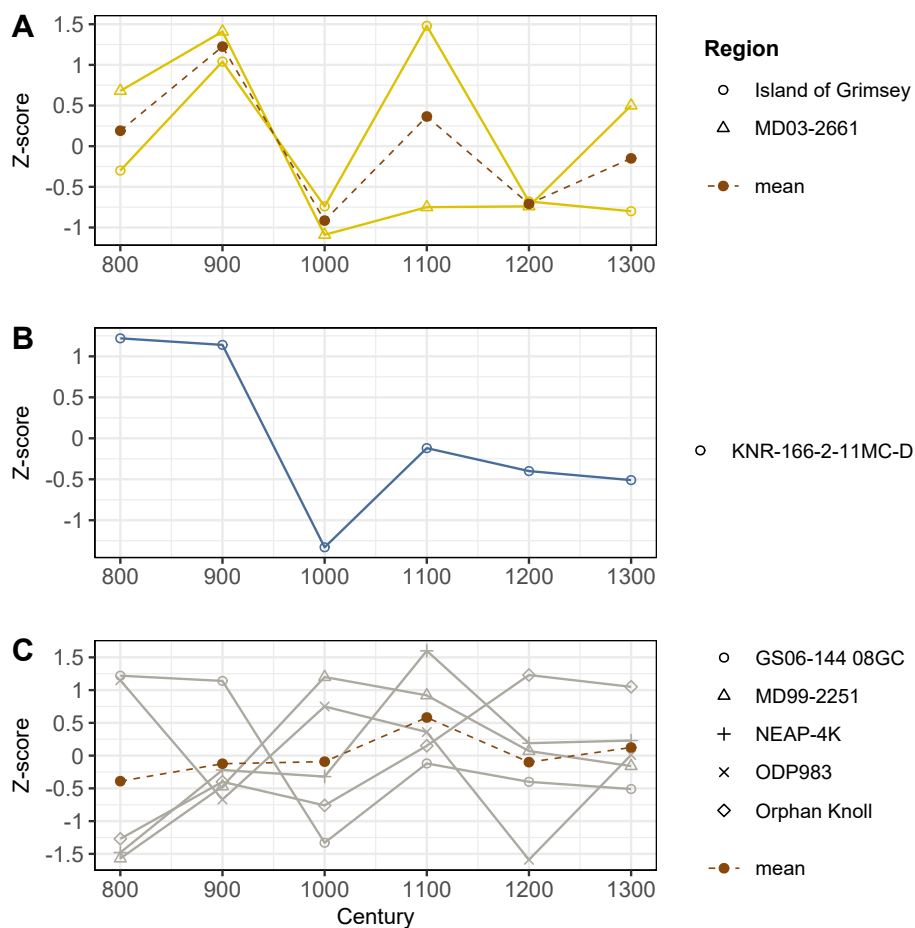
Figure 2. State of AMOC in the North Atlantic regions. Variations in δ^{13}C (A), Cd/Ca ratio (B), and sortable silt (C). The mean reflects the comprehensive average of all records.
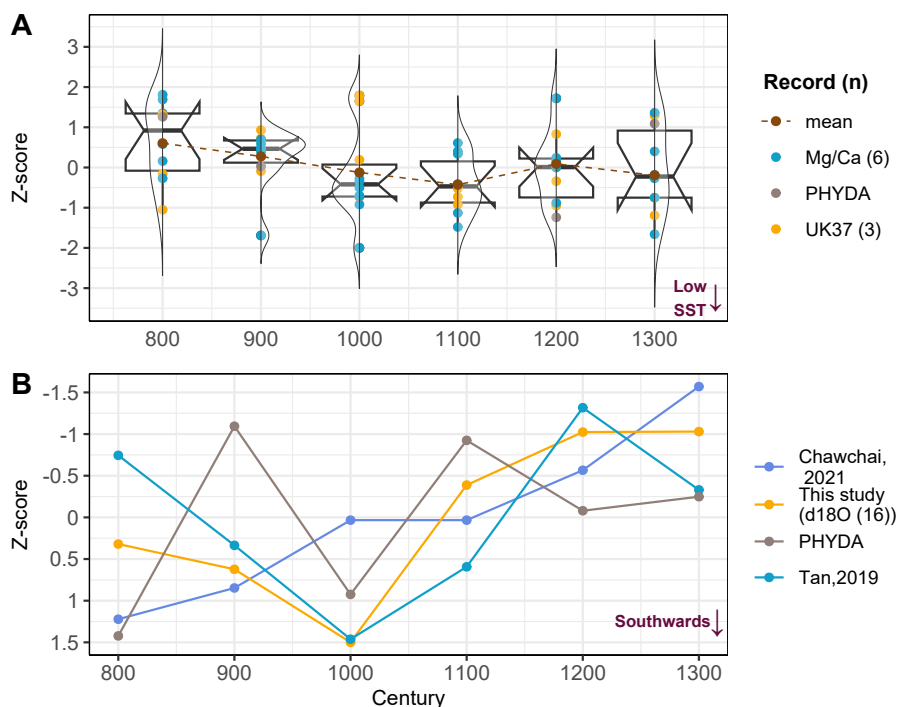
Figure 3. SST (A) and ITCZ (B) conditions over North Atlantic. Positive values for ITCZ indicate a southward shift and negative values suggest a northward shift. The 'Record (n)' denotes the proxy and the number of proxies employed for the analysis.

3.2 Mean temporal patterns of hydroclimates

While observing hydroclimate conditions across Europe at a continental scale, we show that temperature records reveal warm conditions until the 11th century, followed by cold conditions until the 14th century (Figure 4-A). Conversely, precipitation patterns at the continental scale suggest predominantly wet conditions until the 10th century (Figure 4-B). After this period, although variations in precipitation persist, they tend to fluctuate around their centennial mean values, consistently remaining below that centennial mean. The continental scale analysis suggests a correlation between warm climates and wet conditions, while cold climates correspond to dry conditions (Figure 4) . However, at the regional level (Figure 6), hydrological conditions appear to be more closely influenced by variability in ocean-atmospheric circulation, local thermodynamic changes, and the availability of water sources (Chen et al., 2019; Pratap and Markonis, 2022).

Our analysis of the CI distribution (Figure 4-A and B) highlights the complexity and heterogeneity of climatic responses. For temperature (Figure 4-A), the analysis reveals notable variations across the centuries. In the 10th century, there is a warming trend, but the change is not statistically significant as the confidence intervals (CIs) overlap with those of adjacent centuries. Conversely, the mid-11th century exhibits a pronounced shift towards colder values, with the CI not overlapping with those of preceding centuries, indicating a significant cooling event during this period. In the case of P-E conditions (Figure 4-B), the CIs indicate relatively stable conditions from the 10th to the 13th century. However, significant changes occur in the 9th

210 and 12th centuries. The 9th century shows a shift towards drier conditions, with the CI not overlapping with those of adjacent centuries, highlighting a significant drying trend. The 12th century, however, shows a shift towards wetter conditions, with the CIs slightly overlapping with those of the adjacent centuries, suggesting this change is not statistically significant.
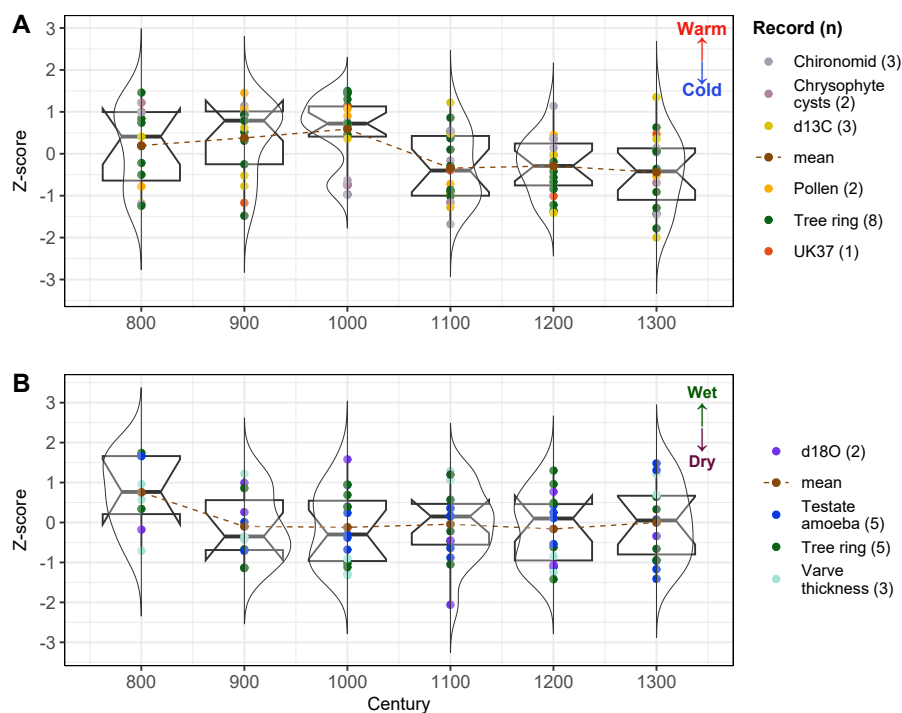
Figure 4. Overview of temperature (A) and P-E (B) conditions over Europe. The 'Record (n)' denotes the proxy and the number of proxies employed for the analysis.

In North America, continental-scale temperatures present a different climate trend compared to Europe: from the 9th to the late 11th centuries, average conditions were warm, followed by the onset of cold climate from the 12th century (Figure

215 5-A). Concerning precipitation, from the 9th to the late 11th century, average hydrological conditions appeared dry, with the precipitation remaining slightly below their centennial mean (Figure 5-B). However, since the 12th century, hydrological conditions appear to be normal, i.e., equal to the centennial mean, while from the 13th to 14th century, there are signals of wet conditions.

The analysis of temperature CIs (Figure 5-A) indicates consistent temperature conditions from the 8th to the 13th century.

220 However, a distinct shift in temperature is observed in the 14th century, suggesting a transition towards colder conditions. Notably, the CIs for this century do not overlap with those of preceding centuries, underscoring a statistically significant change in temperature. For P-E records (Figure 5-B), the CIs around the mean indicate general stability with some variability from the 8th to the 13th century. However, a significant shift occurs in the 14th century, indicating drier conditions, as evidenced by the non-overlapping CIs compared to previous centuries. This transition is marked by a pronounced shift in the P-E distribution

225 towards more negative values, suggesting a significant decrease in P-E availability. This shift indicates a prolonged drying trend that aligns with broader regional climatic changes. The significant change in P-E conditions is underscored by the non-overlapping CIs, reflecting a clear and statistically significant shift in the climatic regime. Overall, the CIs for temperature and P-E conditions in both Europe and North America reveal substantial climatic fluctuations during the 14th century. These fluctuations are marked by pronounced cooling and drying trends.
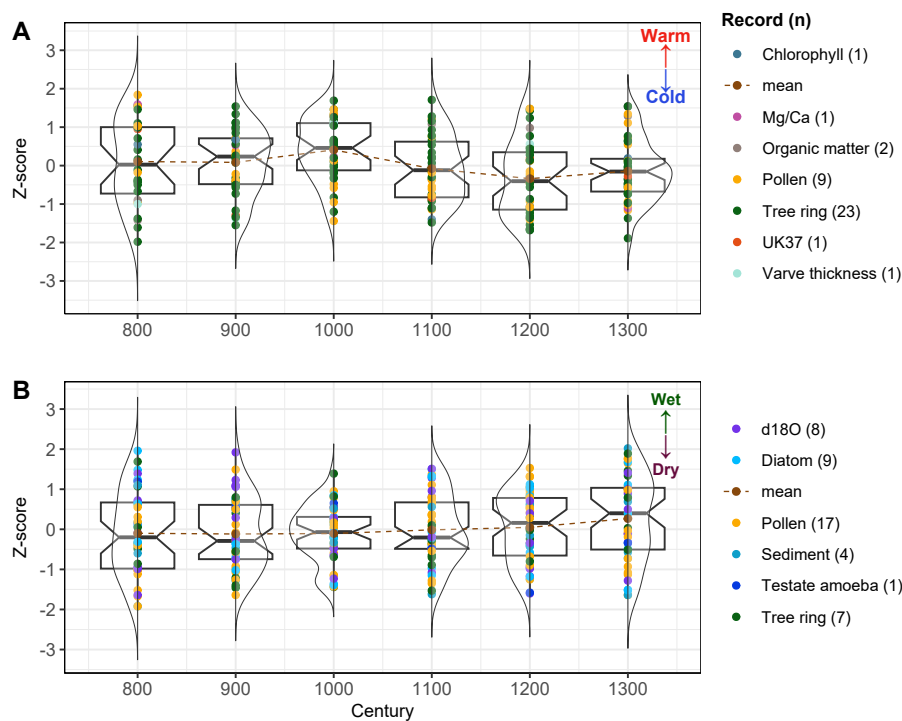
Figure 5. Overall view temperature (A) and P-E (B) conditions over North America. The 'Record (n)' denotes the proxy and the number of proxies employed for the analysis.

3.3 Spatiotemporal patterns of hydroclimates

Spatiotemporal analysis over Europe indicates that most regions experienced warm conditions during the 10th and 11th centuries. This warm climate was followed by colder climates from the 12th to the 14th centuries and wet conditions during the 9th century. However, we observed heterogeneous signals of P-E across subsequent centuries at the centennial scale, potentially attributable to spatial heterogeneity (Figure 6). Notably, our results highlight the 11th century as a period characterized
235 by relatively higher temperatures of MCA. A shift towards colder conditions commenced in the 12th century, prevailing across Europe throughout the 12th to 14th centuries.

Regarding hydroclimate shifts across Europe, our findings unveil a notable latitudinal shift in temperature patterns, particularly from the 12th to the 14th centuries (Figure 6-A). This shift is characterized by the migration of cold climates from

high-latitudes to mid-latitudes. As a result of this latitudinal temperature shift, during the 14th century, most central European
240 regions became even colder than in previous centuries. During the transition from the MCA to the LIA, specifically between
the 13th and 14th centuries, the majority of northern and south-western regions, on average, experienced cold conditions. How-
ever, hydrological conditions reveals a complex hydroclimatic scenario during this transitional period. Notably, over Central
Europe and a few southern areas like the northern Aegean region shifted toward humid conditions (Figure 6-B). During the
central period of the MCA, specifically the 10th and 11th centuries, our analysis demonstrates a warm climate. Nevertheless,
245 in terms of regional hydrological conditions, there is spatial variability, with certain regions experiencing wet conditions while
others depict arid conditions.

In summary, our observations suggest that during the MCA, coastal regions of Europe mostly experienced humid conditions,
except for the 10th and 11th centuries, while inland areas were predominantly arid. For the transition from the MCA-LIA, our
findings uncover a complex hydroclimatic scenario. While some records suggest a cold and arid climate in northern areas,
250 contradictory evidence points to a cold and humid climate regime in southern and western regions.
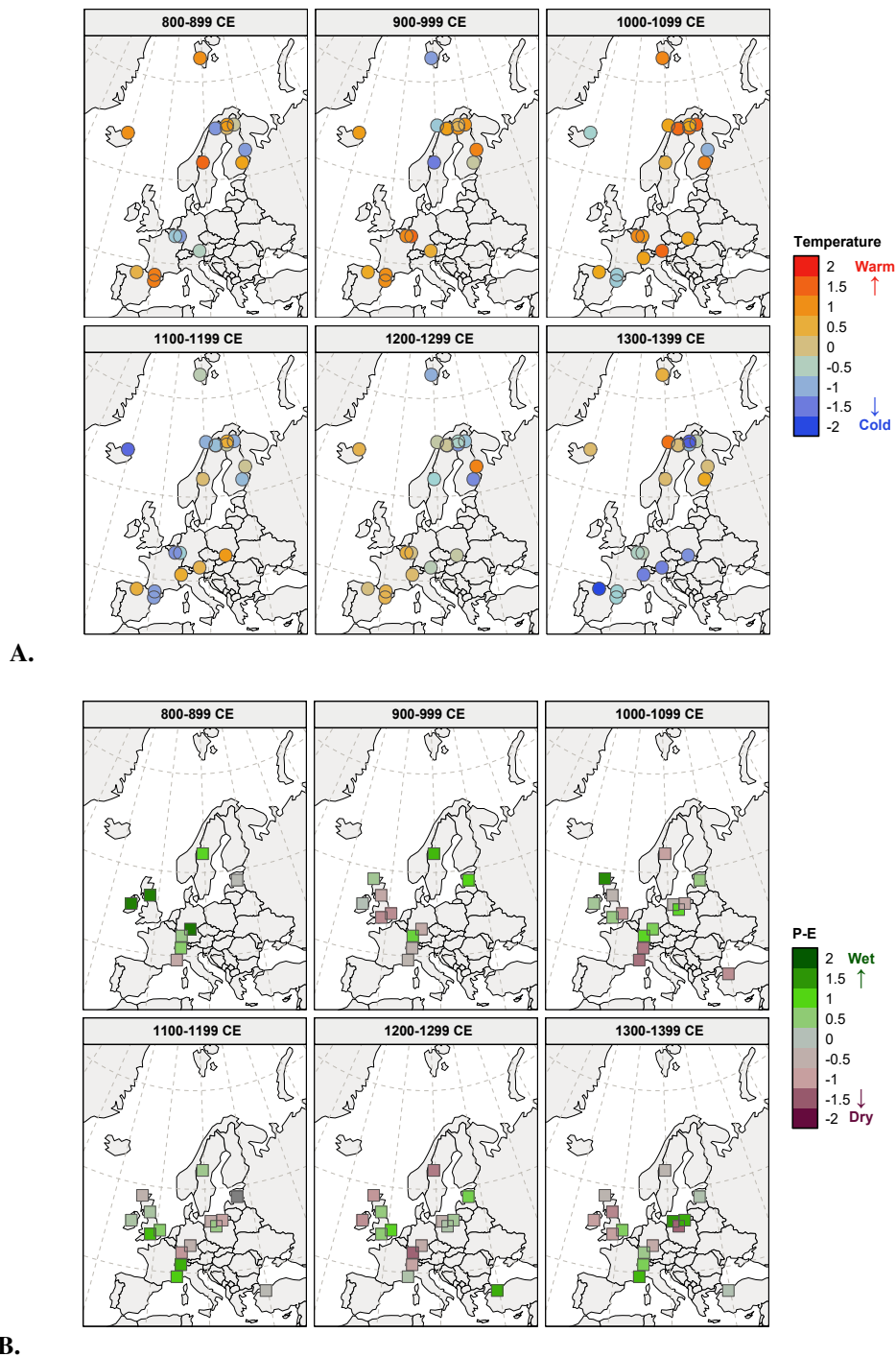
Figure 6. Proxy-estimated temperature (A) and P-E (B) conditions across Europe. The color scale values represent the z-scores.

For North America, the analysis of temperature distributions in high and mid-latitude regions revealed a predominantly warm climate during the 9th and 11th centuries (Figure 7), albeit with some regions displaying cold conditions as well. Commencing from the 12th century, a transition towards cooler climate began prevailing in high and mid-latitude regions. Initially, this change was most pronounced in coastal areas and gradually extended further inland. More specifically, the onset of cold

255 climates was observed in eastern North America and gradually extended to central and western regions between the 12th to the 14th centuries. In our examination of regional-scale hydroclimate variability, we noted a recurring cyclical pattern of dry and wet conditions at a centennial scale in the northern part of British Columbia. Dry conditions were evident in the 9th, 11th, and 13th centuries, while wet conditions prevailed during the 10th, 12th, and 14th centuries. In certain regions like the north of Alberta, our observations indicated a dry climate when the temperature was warm but close to its centennial mean. However,

260 as the climate became even warmer, these areas exhibited a wetter climate.

Hydrological conditions in high and mid-latitude regions exhibited spatial and temporal heterogeneity, with some areas showing humid responses to warm conditions while others experienced arid conditions. This complex spatial pattern of hydrological response persisted during the cold climate phases, with most regions being arid and some remaining humid. Overall, hydroclimate patterns during the MCA in North America included all the possible hydroclimatic combinations, i.e., as warm-

265 humid, warm-arid, cold-humid, and cold-arid regimes. Our findings imply that arid hydrological conditions in North American regions coincided with periods when temperatures exceeded their centennial-scale averages, whereas humid conditions were more prevalent when temperatures were close to or aligned with their centennial-scale averages.
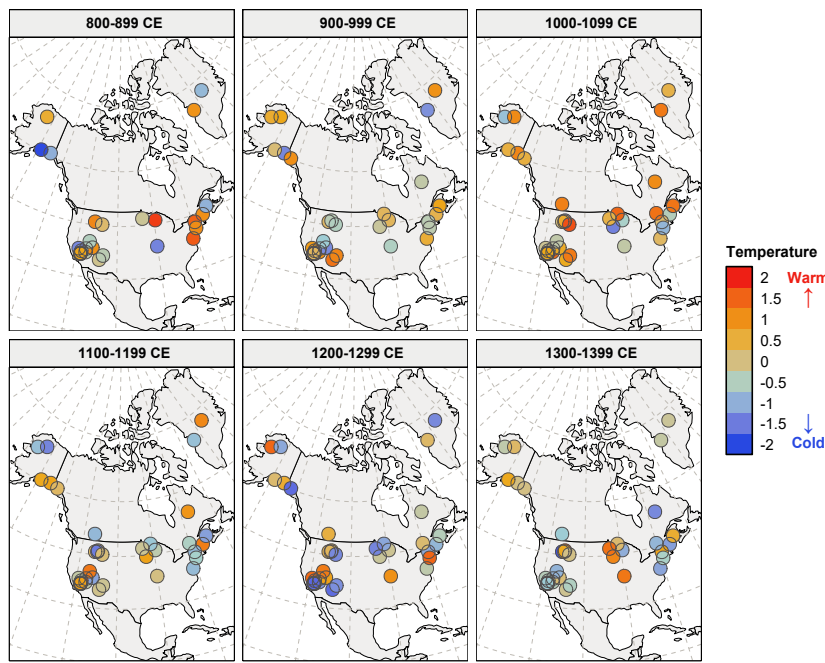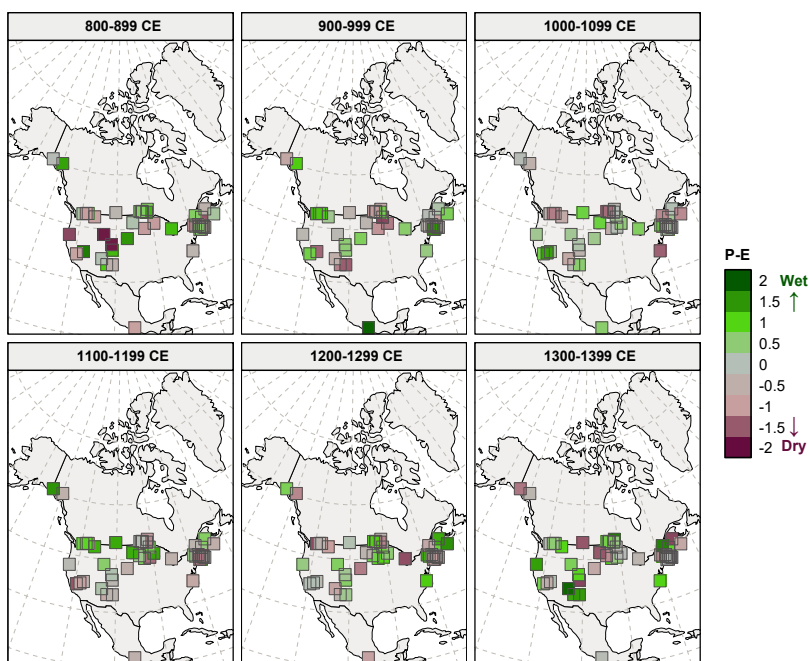
Figure 7. Overview of temperature (A) and P-E (B) conditions over North America. The color scale values represent the z-scores.

3.3.1 Comparative assessment of outcomes from proxy and model assimilation

The comparison between proxy and model outputs offers valuable insights for accurately constraining future hydroclimatic
270   conditions using climate model projections. Therefore, this study compared proxy results with model assimilations, specifically
PHYDA and Paleoview, as shown in Figure 8(A, B). We categorised the model assimilations into two types of outputs: point
and grid. The point output represents values at the precise locations of the proxy data, while the grid output presents average
conditions across the continent.

We observed that both PHYDA and Paleoview assimilations indicate warmer climatic conditions from 9th to mid-11th
275   century, while PHYDA is overestimating the temperature conditions over a continental scale at grid scale (Figure 8). Our
analysis shows that temperatures provided by Paleoview both at grid and point levels across high and mid-latitudes align
closely with the trends observed in proxy records. In contrast, temperatures modelled by PHYDA align well with proxy-data at
grid scale, but opposing trend beginning from the 9th century in high-latitudes are observed at the point scales. At mid-latitudes,
both PHYDA grid and point data show an underestimation of temperature compared to the proxy records.

280   Both the proxy data and model assimilation (particularly the PHYDA grid and Paleoview point) indicated predominantly arid
conditions at high-latitudes. This aridity is particularly notable from the mid-10th to the late-11th century in the PHYDA grid
assimilation and extends until the mid-13th century in the Paleoview point assimilation. However, discrepancies arise, with both
PHYDA point- and Paleoview grid-scales showing humid conditions at high- and mid-latitudes from mid-10th to the mid-11th.
Additionally, at mid-latitudes, differences between the proxy and PHYDA assimilation become evident. PHYDA assimilation
285   suggest humid conditions from the 10th to mid-12th century, while the proxy data suggests arid conditions. Simultaneously,
Paleoview is showing an underestimation for arid conditions.

In summary, our comparison reveals divergent trends in model assimilation under similar climate conditions. Paleoview
indicates that warm climates tend to promote humid conditions at high and mid-latitudes. PHYDA, on the other hand, suggests
that warm climates result in arid conditions at high-latitudes and humid conditions at mid-latitudes. At the grid scale, both
290   models generally satisfactorily reproduce climatic conditions at mid and high-latitudes. However, at regional scale, some
discrepancies arise, possibly due to model biases or high uncertainty and/or limited availability of data for model assimilation
in those specific regions.

Europe
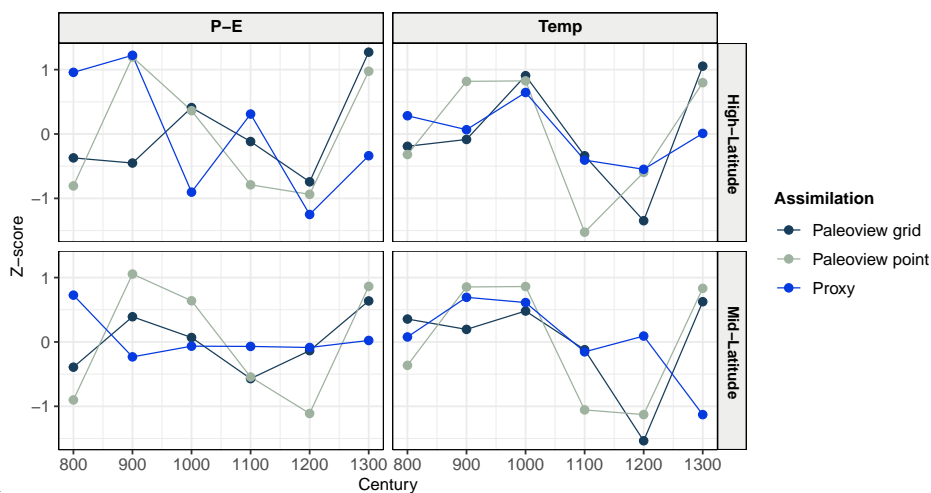
A. Paleoview
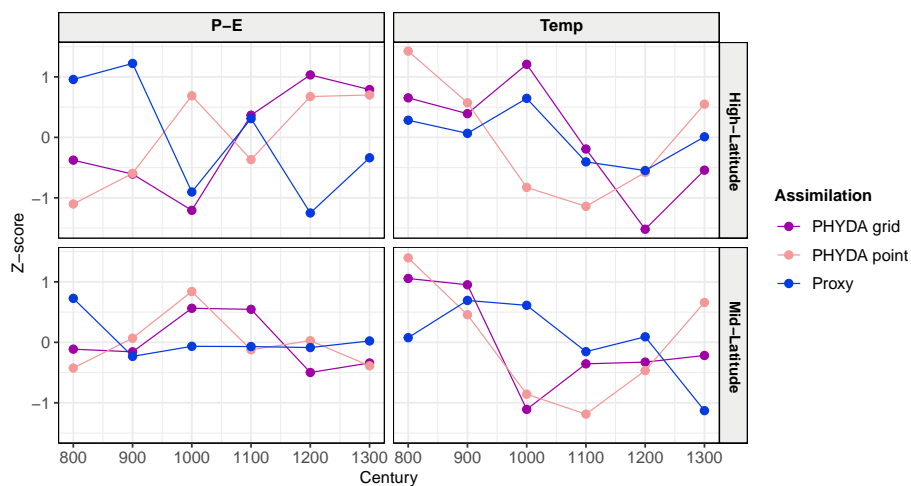
B. PHYDA

Figure 8. Evaluation of model (Paleoview (A), PHYDA (B)) and proxy estimated precipitation (P-E) and temperature (Temp) conditions over Europe. The model point represents the exact location of proxy data.

Figure 9 presents the results of our temporal variability assessment using both proxy data and model assimilation over North America. At point scale, both models exhibit a pattern similar to proxy records. However, the models either over-
or underestimate temperature and precipitation. Data-Model discrepancies become apparent, particularly at grid scales. For instance, lower temperatures and higher precipitation are observed in Northeastern America from the 9th to the 12th century. By contrast, western regions exhibit lower temperatures and lower precipitation during this period. After the 12th century, lower/higher temperatures are associated with reduced precipitation over both eastern and western North America. At point

scale, model output show a modest agreement with proxy data. Temperature simulated by both PHYDA and Paleoview in
300   eastern and western North America align with the proxy data, with higher temperatures during the 10th to late 11th century.

However, we noticed that both proxy data and model assimilation depict a shift from a warm to a cold state, specifically
after the 11th century. In terms of precipitation, both PHYDA and Paleoview diverge from the proxy data. While the proxy
data suggests below-average (centennial-scale) precipitation between the 10th to late 11th centuries, both model assimilation
indicate an increase during this period. In some cases, the proxy and model point data align well, whereas the model results
305   at the grid scale deviate from data estimates. This discrepancy underscores the presence of substantial uncertainties in the
proxy and model point data, potentially arising from limited data availability or measurement errors. The notable uncertainty
in the model assimilation highlights the importance of refining the models and reducing measurement errors to enhance our
understanding and prediction of hydroclimate variability.

Climate
of the Past
Discussions
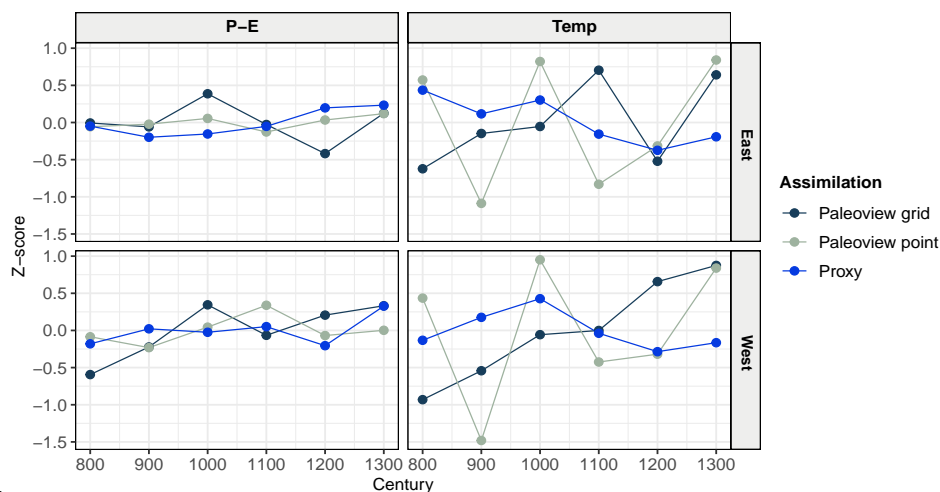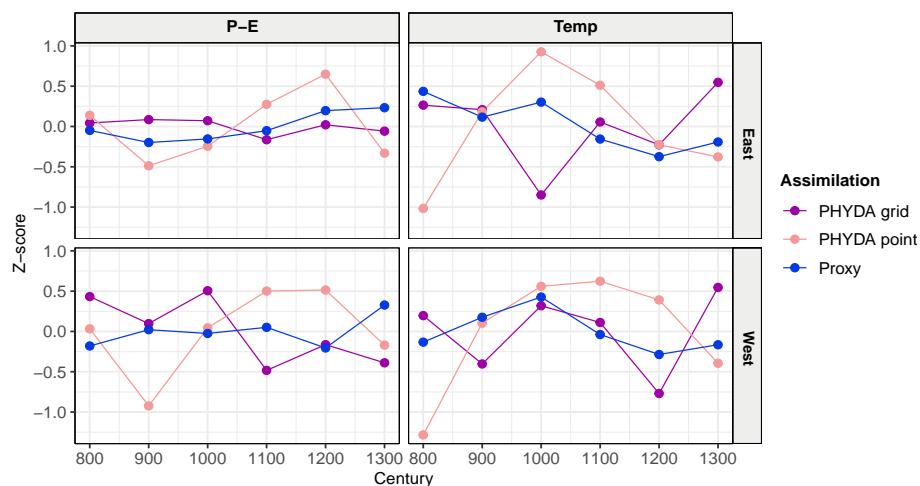
Figure 9. Evaluation of model (Paleoview (A), PHYDA (B)) and proxy estimated precipitation (P-E) and temperature (Temp) conditions over North America. The model point represents the exact location of proxy data.

The comparison between model assimilations and proxy data reveals variability in correlations depending on the variable
310 and region (Table 1). For P-E, a significant/strong correlation is observed between PHYDA points and proxy data over Europe, while all other comparisons exhibit low/non-significant correlations. For temperature, correlations are generally low/non-significant across all comparisons. For North America, both P-E and temperature variables show non-significant correlations across all proxy and model comparisons. These results underscore the challenge of achieving better agreement between model assimilations and proxy data, highlighting the need for improvements in model performance.

Climate
of the Past

Discussions

Table 1. Correlations between proxy and model assimilations in terms of R^2 and p-values.

Continent	Comparison	Variable	R^2	p value
Europe	Proxy vs PHYDA grid	P-E	0.09	0.35
Europe	Proxy vs PHYDA point	P-E	0.68	~0
Europe	Proxy vs Paleoview grid	P-E	0.06	0.44
Europe	Proxy vs Paleoview point	P-E	~0	0.94
Europe	Proxy vs PHYDA grid	Temp	0.19	0.15
Europe	Proxy vs PHYDA point	Temp	~0	0.99
Europe	Proxy vs Paleoview grid	Temp	0.05	0.49
Europe	Proxy vs Paleoview point	Temp	0.09	0.34
N.America	Proxy vs PHYDA grid	P-E	0.18	~0
N.America	Proxy vs PHYDA point	P-E	~0	0.99
N.America	Proxy vs Paleoview grid	P-E	0.01	0.77
N.America	Proxy vs Paleoview point	P-E	0.09	0.36
N.America	Proxy vs PHYDA grid	Temp	~0	0.97
N.America	Proxy vs PHYDA point	Temp	0.02	0.66
N.America	Proxy vs Paleoview grid	Temp	0.14	0.24
N.America	Proxy vs Paleoview point	Temp	0.04	0.54

4 Discussion

4.1 State of the North Atlantic during the MCA

The state of the North Atlantic plays a pivotal role in shaping hydroclimate patterns across globe. In this study, we focused on key factors including the AMOC and SST conditions during the MCA period to characterize the state of the North Atlantic. Various modelling studies have suggested a weakened response of the AMOC to warm climate conditions (Dima et al., 2021; Cini et al., 2024). However, our investigation did not find any evidence of AMOC weakening in response during the warmer MCA (Latif et al., 2022). Although we selected various (indirect) AMOC proxies from different locations across the North Atlantic Ocean, determining the AMOC condition during the warm climate remains challenging. It is possible that the AMOC underwent changes during that time, but the signal may have been too weak to be captured by the selected proxies. The proxy-records we selected exhibit two distinct responses. Six records show a seemingly weaker AMOC during the 10th and 11th century, while two records show the exact opposite. Even within similar proxies (e.g., sortable silts, Figure 2.C), the data-spread is very large and prevents us to draw any clear picture of temporal AMOC changes during the MCA. Definitive conclusions on the sensitivity of AMOC tracers across both space and time require further investigation.

Sea Surface Temperatures (SSTs) (Figure 3.A) were consistently higher over the North Atlantic region from the 9th to the mid of 10th century. Low SST are observed during the mid-10th to 14th centuries, which may be related to a strengthening of the Subtropical high-pressure system over the North Atlantic (Gibson et al., 2024). In addition, freshwater discharge into the North Atlantic could have also played a role in reducing the SST in the region (Schmidt et al., 2004; Levy et al., 2023). Low SST in the North Atlantic Ocean may have triggered a shift of the ITCZ towards the southern hemisphere (Steinman et al., 2022;

Giannini et al., 2000), particularly during the 10th and 11th centuries. These oceanic influences likely reshaped atmospheric circulation and dynamics over the North Atlantic region, expanding colder climate regions and constraining moisture flux

335 across North America and Europe (Frankignoul and Kestenare, 2005), in particular between the 12th and 14th centuries.

4.2 Relationships between SSTs and hydroclimates in the north Atlantic region

The variations in SSTs in the North Atlantic Ocean are known to significantly influence regional climates in Europe and North America (Czaja and Frankignoul, 2002; Jones and Anderson, 2008). We observed a link between the warm climate of Europe and high North Atlantic SST, particularly during the onset of the MCA. It is noticed that high SSTs are potentially linked with

340 a positive phase of the North Atlantic Oscillation (NAO) and intensified westerlies (Delworth and Greatbatch, 2000; Hurrell and Deser, 2010; Kim et al., 2023). It is plausible that the positive phase of the NAO and enhanced westerlies facilitated the redistribution of atmospheric heat across both continents, thereby contributing to the warm conditions observed (Trouet et al., 2009). However, we observed that as SST began to decrease from the mid-10th century, transitioning to a lower state, the warm climate also shifted towards a colder climate across Europe and North America. This decline in SST, hindering northward

345 meridional heat flow, further contributed to a weakened NAO and westerlies (Lehner et al., 2013).

Furthermore, this variability in SST and westerlies would have played a significant role in European hydroclimate variability. The low (high) SST influenced the transport of cold (warm) air by weaker (stronger) westerlies to western and southern European regions, thereby causing cold (warm) and arid (humid) climates (Trouet et al., 2009), respectively. We speculate that the cooling of the North Atlantic Ocean observed from the mid-10th to the 14th century, likely due to low SST, led to

350 a reduction in moisture flux and decreased temperatures towards European regions. This decrease in moisture flux from the ocean source and consequent cold climate may have contributed a spatially diverse pattern of precipitation across Europe, characterized by both wet and arid conditions (Liu et al., 2020). However, it is important to note that this spatially diverse pattern of precipitation across Europe may have also been influenced by regional thermodynamic responses due to changes in ocean-atmospheric circulation (Pratap and Markonis, 2022).

355 Besides Europe, hydroclimate variability in the North American region likely responded to centennial-scale fluctuations in SST (Cook et al., 2022). The warm conditions observed over North America during the MCA may be associated to intensified heat transport facilitated by strengthened westerlies, influenced by the high North Atlantic SST condition. Furthermore, during the 9th to mid-10th centuries, the high SST may have contributed to a positive feedback mechanism (water vapour feedback). These high SSTs and the resulting positive feedback mechanism conditions likely led to arid or drought-like conditions in

360 western and southern North America (Seager et al., 2007), while the northwestern regions experienced increased humidity during that period. The arid conditions are likely linked to episodes of drought, which have also been observed and documented by Cook et al. (2014) and Chen et al. (2021).

However, as discussed earlier, by the mid-10th century, the SST began decreasing, leading a reduced atmospheric moisture supply to eastern and other parts of North America. This, in turn, led to reduced precipitation and drought-like conditions in

365 these regions (Seager et al., 2008). Mainly, during the MCA, western and central regions of North America experienced warm and arid climatic conditions, characterized by decadal or centennial-scale megadrought events (Oglesby et al., 2011). While

the underlying factors behind these megadrought events are still under investigation, our findings suggest that these drought conditions in North America may have been linked to a southward shifting ITCZ in response to low SST. This shift likely constrained the moisture supply over these regions.

370   The precise forcing of hydroclimates during the MCA in North America remain subject to ongoing debate. Notably, the climatic conditions in North America appear significantly influenced by North Atlantic Ocean fluctuations (Hurrell and Deser, 2010). Our study also suggests an agreement on a relationship between warm North Atlantic Ocean conditions and hydroclimate variability over North America. Proxy observations revealed spatially distinct precipitation patterns across North America. We found that coastal areas generally experienced increased precipitation when temperatures were close to their centennial-

375   scale means, while arid climates were associated with temperatures exceeding this mean. By contrast, more inland regions experienced higher precipitation when temperatures were high. We show that both in eastern and western North America, lower (higher) temperatures were associated with more arid (humid) conditions. These results suggest that variations in temperature influenced precipitation patterns across the continent.

4.3   Potential drivers of hydroclimate changes over North America and Europe

380   Temperature and precipitation are integral components of the hydroclimate system. Many studies have emphasized the high sensitivity of hydroclimate patterns in Europe to fluctuations in North Atlantic oceanic circulation, with documented occurrences of recurrent drought-like conditions during the MCA (Helama et al., 2009; Hernández et al., 2020). However, the validation and reliability of hydroclimatic records from the MCA in Europe, particularly regarding the origins of drought-like conditions, are uncertain and sometimes contradictory, necessitating further verification (Seager et al., 2007; Carrillo et al.,

385   2022). We hypothesize that the warm climate of the MCA might have resulted in increased temperatures in the Arctic regions (Mann et al., 2009), potentially enabling the influx of atmospheric moisture. This, in turn, could have resulted in a humid climate in northwest Europe, particularly during the 11th and 13th centuries. On the other hand, the prolonged warm climate spanning over three centuries (from the 9th to the 11th centuries) likely exerted a significant influence on the climate dynamics of the Arctic regions (Bindoff et al., 2013). This led to the melting of ice sheets, glaciers, and sea ice, resulting in a substantial

390   influx of freshwater into the North Atlantic Ocean. This change over the North Atlantic Ocean potentially established a linkage between the MCA-LIA transition and hydroclimate fluctuations across North America and Europe (Holliday et al., 2020).

The influx of low-density freshwater may have impacted deep ocean convection by reducing density in the Labrador Sea, resulting in the cooling and freshening of the North Atlantic Current (Robson et al., 2014). These changes in the North Atlantic Ocean notably regulated the state of the SST and the position of the ITCZ in the North Atlantic region. Specifically, cooling

395   and freshening led to low SST, which likely characterized the emergence of the MCA-LIA transition (Trouet et al., 2012). Most likely, the low SST over the North Atlantic ocean would have constrained the northward movement of warm tropical water, resulting in the development of an SST gradient (Bond et al., 2001). Consequently, the increased SST gradient over the North Atlantic probably restricted the transport of atmospheric heat and moisture from the tropics (Srokosz and Bryden, 2015), contributing to the southward shift of the ITCZ (Giannini et al., 2000). On the other hand, the abrupt cold climate that

400 occurred after the 13th century, known as the LIA, may have been a response to the prolonged low SST and southward ITCZ (Lynch-Stieglitz, 2017).

Notably, during the warm phases of the MCA, we observed warm conditions coinciding with high SST and a northward shift in the ITCZ. Throughout this period, continental-scale hydroclimate displayed warm and wet conditions across both continents. However, after the peak warmth of the MCA (i.e., after 11th century), the state of SST and ITCZ underwent divergent

405 shifts–transitioning from high to low and northward to southward, respectively. Concurrently, continental-scale hydroclimate patterns over North America and Europe also shifted. Notably, after 11th century, temperatures shifted from warm to cold, and hydrological conditions transitioned from wet to dry. In the meantime, at a regional scale across both continents, temperature changes appeared associated with shifts in the North Atlantic state, while precipitation patterns remain uncertain. Regional precipitation distribution seems more linked to specific changes in the local climate system, particularly in response

410 to thermodynamic shifts. In specific, the occurrence of humid or arid conditions in certain locations across Europe and North America could be associated with localized responses to amplified regional atmospheric warming (Tabari, 2020). However, further investigations are needed to confirm the precise response of hydrological conditions in a warm climate.

In summary, our observations indicate that variations in SST and ITCZ exert a significant influence on hydroclimate distributions, as the variability in both appears to shift in parallel. These variations in the North Atlantic state impact ocean-

415 atmospheric-land circulation patterns, thereby constraining the distribution of terrestrial moisture and heat, which contribute to shaping the hydroclimate.

4.4 Proxy and model assimilation comparison

When comparing model assimilation (PHYDA and Paleoview) with proxy outcomes, we observed significant discrepancies between them. The uncertainties in both proxy and model outcomes may depend on several key factors. For instance, proxies

420 are often spatially unevenly distributed and capture localized climate variations, which may not fully represent broader climate dynamics. Conversely, models introduce biases through the simplification of physical processes and assumptions embedded in parameterizations, especially when simulating complex regional dynamics. These limitations complicate direct comparisons of proxy with climate models, which simulate conditions over comprehensive grids.

On the other hand, the discrepancies between grid- and point-based outcomes over both European and North American

425 regions may also be attributed to several factors. For instance, climate model grids average climate conditions over large areas, which can mask the fine-scale processes that are captured well by regional proxies. In Europe, specially over high- and mid-latitude regions temperature and precipitation distribution are significantly influenced by different climatic drivers, such as polar jet streams and mid-latitude cyclones, which may be inadequately represented in models but more accurately reflected in proxy records (Woollings, 2010; Studholme et al., 2022). Similarly, temperature and precipitation variability over the east-

430 west contrast in North America arises from distinct climatic regimes: the west is dominated more by oceanic influences and orographic effects, while the east experiences greater continental variability (Trenberth et al., 2007). Proxies capture these localized signals, whereas models often generalize them, which can lead to discrepancies in regional climate dynamics.

In conclusion, our findings reveal that while both models generally align with proxy trends at the grid scale, notable discrepancies emerge at the regional level. Paleoview tends to associate warmer climates with humid conditions, while PHYDA
435   indicates arid conditions at high latitudes. These divergent trends underscore the importance of careful model selection and the need for improved data availability to enhance future hydroclimatic projections.

5   Conclusions

This study investigates centennial-scale hydroclimate patterns across Europe and North America during the MCA, aiming to uncover potential connections between these patterns and the North Atlantic variability (in SST, AMOC, and the ITCZ) within
440   a warm climate context. Although the state of the AMOC during warm climates remains uncertain, we found that centennial-scale variability in SST and ITCZ dynamics played a pivotal role in shaping hydroclimate patterns across both continents and in the transitional shift from the MCA to the LIA. This transitional period witnessed a shift in hydroclimate across North America and Europe, transitioning from warm to cold and wet to dry climates, with persistent uncertainties in hydrological conditions. During the warm climate, hydroclimate changes and their link with the North Atlantic variability demonstrate a
445   lead-lag relationship, notably prominent in temperature variations. Our interpretation of a lead-lag relationship is rooted in the alignment between a warm climate and a strengthened North Atlantic condition, which later transitioned to weaker states, potentially due to increased input of freshwater from Arctic melting and sea ice.

We anticipate that variations in the North Atlantic, including SST and the ITCZ, may have acted as possible factors in altering hydroclimate patterns at the continental scale. Specifically, low SST and southward shifting ITCZ. This led to cold and
450   arid hydroclimate conditions across Europe and North America, particularly after the 11th century. This transition may have played a significant role in initiating the LIA (Trouet et al., 2009; Wanamaker et al., 2012). When considering the interplay between temperature and precipitation, it is crucial to acknowledge the complexity and spatial variability of their relationship. Our study provides a comprehensive overview, revealing that during the MCA, elevated temperatures exceeding the centennial scale average were generally associated with arid climates. Conversely, slightly warmer conditions than the centennial average
455   tended to coincide with more frequent occurrences of humid conditions. Additionally, our investigation observed that increased precipitation under low temperatures was sporadic, possibly indicating regional climate heterogeneity.

Overall, our findings underscore the significant modulation of hydroclimate variability during the MCA due to North Atlantic variability, particularly in SST and shifts in the ITCZ. This North Atlantic modulation influenced the redistribution of atmospheric heat and water vapor, thereby shaping the hydroclimate across the Northern Hemisphere. Based on the evidence
460   from the MCA, it is plausible to consider that ongoing climate warming may contribute to the future lowering in SST and a southward shift in ITCZ. Consequently, this may result in a similar hydroclimate shift as observed during the MCA. However, the intricate relationship between hydrological variability and its latitudinal heterogeneity, particularly under warmer climate conditions, remains enigmatic and warrants further in-depth investigation.

Data availability. The data used in this study are open-source and publicly available on the website of NOAA's National Centers for Environ-
465 mental Information (https://www.ncei.noaa.gov/products/paleoclimatology) and the Past Global Changes (PAGES) (https://pastglobalchanges.
org/science/data/databases).

Appendix A: Data tables

Table A1. Source and distribution information for precipitation (Precip) and temperature (Temp) across the European region.

Region	Material	Fractions	Proxy	Variable	Age uncertainty (years)	Latitude	Longitude	Investigators	Publication
North Aegean	Tree	Tree-rings	Total ring width	Precip		40.5	29.5	Griggs et al., 2007	https://doi.org/10.1002/joc.1459
Central and Eastern Pyrenees	Lake sediment	Sediment	Chrysophyte cyst	Temp		41.5	0.75	Pla et al., 2004	https://doi.org/10.1007/s00382-004-0482-1
Lake Redon	Lake sediment	Sediment	Chrysophyte cyst	Temp		42.64	0.77	Pla et al., 2004	https://doi.org/10.1007/s00382-004-0482-1
Northern inland Iberia	Stalagmite	Stalagmite	δ^{13}C	Temp	± 5	42.69	-3.94	Martín-Chivelet et al., 2011	https://doi.org/10.1016/j.gloplacha.2011.02.002
Lake Allos	Lake sediment	Sediment	Varve thickness	Precip	± 30	44.25	6.72	Wilhelm et al., 2012	https://doi.org/10.1016/j.yqres.2012.03.003
Seebergsee	Lake sediment	Chironomid	C-assemblage	Temp	±12	46.12	7.47	Larocque et al., 2012	https://doi.org/10.1016/j.quascirev.2012.03.010
Lake Oeschinen	Lake sediment	Sediment	Varve thickness	Precip	± 9	46.5	7.73	Amann et al., 2015	https://doi.org/10.1016/j.quascirev.2015.03.002
Alps	Tree	Tree-rings	Total ring width	Temp		47.5	12.5	Büntgen et al., 2016	https://doi.org/10.1038/ngeo2652
Upper Rhine Valley	Tree	Tree-rings	Total ring width	Precip		48.75	7.75	Tegel et al., 2020	https://doi.org/10.1038/s41598-020-73383-8
Tatra region	Tree	Tree-rings	Total ring width	Temp		49.5	20	Büntgen et al., 2013	https://doi.org/10.1073/pnas.1211485110
Main River Region	Tree	Tree-rings	Total ring width	Precip		50.05	10.2	Land et al., 2019	https://doi.org/10.5194/cp-15-1677-2019
Meerfelder Maar	Lake sediment	Pollen	P-assemblage	Temp		50.1	5.5	Litt et al., 2009	https://doi.org/10.1111/j.1502-3885.2009.00096.x
Holzmaar	Lake sediment	Pollen	P-assemblage	Temp	± 5	50.12	6.88	Litt et al., 2009	https://doi.org/10.1111/j.1502-3885.2009.00096.x
Southern-Central England	Tree	Tree-rings	Total ring width	Precip		51.6	-1.75	Wilson et al., 2012	https://doi.org/10.1007/s00382-012-1318-z
East Anglia	Tree	Tree-rings	Total ring width	Precip		52.5	1	Cooper et al., 2012	https://doi.org/10.1007/s00382-012-1328-x
Stazki Bog	Peatland sediment	Sediment	Testate amoeba	Precip	± 30	53.42	18.08	Lamentowicz et al., 2010	https://doi.org/10.1016/j.palaeo.2008.04.023
Ireland	Peatland sediment	Sediment	Testate amoeba	Precip		53.5	-8	Swindles et al., 2013	https://doi.org/10.1016/j.earscirev.2013.08.012
Slowinskie Blota	Peatland sediment	Sediment	Testate amoeba	Precip	± 30	54.36	16.49	Lamentowicz et al., 2010	https://doi.org/10.1111/j.1502-3885.2008.00047.x
Stazki Bog	Peatland sediment	Sediment	Testate amoeba	Precip	± 30	54.42	20.08	Lamentowicz et al., 2010	https://doi.org/10.1016/j.palaeo.2008.04.023
Northern Britain	Peatland sediment	Sediment	Testate amoeba	Precip		55.5	-2.75	Charman et al., 2006	https://doi.org/10.1016/j.quascirev.2005.05.005
Uamh an Tartair	Stalagmite	Stalagmite	δ^{18}O	Precip		58.15	-5.98	Baker et al., 2010	https://doi.org/10.1016/j.gloplacha.2010.12.007
Finnish Lakeland	Tree	Tree-rings	Total ring width	Temp		62.33	28.33	Helama et al., 2014	https://doi.org/10.2478/s13386-013-0163-0
Jämtland	Tree	Tree-rings	Total ring width	Temp		63	14.05	Zhang et al., 2016	https://doi.org/10.5194/cp-12-1297-2016
Stora Vidarvatn	Lake sediment	Chironomid	C-assemblage	Temp		66.24	-15.83	Axford et al., 2008	https://doi.org/10.1007/s10933-008-9251-1
Northern Fennoscandia	Tree	Tree-rings	Total ring width	Temp	± 15	68.15	24.38	Matskovsky and Helama, 2014	https://doi.org/10.5194/cp-10-1473-2014
Torneträsk	Tree	Cellulose	δ^{13}C	Temp		68.2	19.8	Loader et al., 2013	https://doi.org/10.1016/j.quascirev.2012.11.014
Torneträsk	Tree	Tree-rings	Total ring width	Temp	± 15	68.26	19.63	Melvin et al., 2013	https://doi.org/10.1177/0959683612460791
Laanila	Tree	Tree-rings	Total ring width	Temp		68.5	27.5	Gagen et al., 2011	https://doi.org/10.1029/2010GL046216
Northern Fennoscandia	Tree	Tree-rings	Total ring width	Temp		68.63	24.69	Helama et al., 2012	https://doi.org/10.1007/s10933-012-9598-1
Forfjorddalen	Tree	Cellulose	δ^{13}C	Temp		68.8	15.73	Young et al., 2012	https://doi.org/10.1007/s00382-011-1246-3
Kongressvatnet	Lake sediment	Sediment	$U^{k'}37$	Temp		78.02	13.93	Andrea et al., 2012	https://doi.org/10.1130/G33365.1
Lake Nuudsaku	Lake sediment	Sediment	δ^{18}O	Precip		58.1969	25.6275	Nathan et al., 2017	https://doi.org/10.1016/j.quascirev.2017.09.013
Lake Storsjön	Lake sediment	Varve	Varve thickness	Precip		63.12	14.37	Labuhn et al., 2017	https://doi.org/10.3390/quat1010002
Kylmanlampi	Lake sediment	Chironomid	C-assemblage	Temp		64.3	30.25	Luoto et al., 2003	https://doi.org/10.3354/cr01331

Table A2. Source and distribution information for precipitation (Precip) and temperature (Temp) across the North American region. (Part-1)

Region	Material	Fractions	Proxy	Variable	Age uncertainty (years)	Latitude	Longitude	Investigators	Publication
Albemarle Sound Drainage Basin	Tree	Tree-rings	Total ring width	Precip		36	-77	Stahle et al., 2011	https://doi.org/10.1007/s12237-013-9643-y
Beaver Lake	Lake sediment	Diatom	D-assemblage	Precip	±35	42.46	-100.67	Schmieder et al., 2011	https://doi.org/10.1016/j.quascirev.2011.04.011
Berry Pond	Lake sediment	Pollen	P-assemblage	Precip		42.51	-73.32	Marsicek et al., 2013	https://doi.org/10.1016/j.quascirev.2013.09.001
Blood Pond	Lake sediment	Pollen	P-assemblage	Precip		42.08	-71.96	Marsicek et al., 2013	https://doi.org/10.1016/j.quascirev.2013.09.001
Bufflehead Pond	Lake sediment	Sediment	GPR	Precip	±40	44.99	-93.54	Shuman et al., 2009	https://doi.org/10.1890/08-0985.1
Castor Lake	Lake sediment	Sediment	$\delta^{18}O$	Precip		48.54	-119.56	Steinman et al., 2012	https://doi.org/10.1073/pnas.1201083109
Chesapeake Bay	Marine sediment	Sediment	Mg/Ca	Temp		38.61	-76.4	Cronin et al., 2010	https://doi.org/10.1016/j.palaeo.2010.08.009
Clear pond	Lake sediment	Pollen	P-assemblage	Temp, Precip		43	-74	Gajewski 1988	https://doi.org/10.1016/0033-5894(88)90034-8
Conroy lake	Lake sediment	Pollen	P-assemblage	Temp, Precip		46.17	-67.53	Gajewski 1988	https://doi.org/10.1016/0033-5894(88)90034-8
Dark Lake	Lake sediment	Pollen	P-assemblage	Precip		45.16	-91.28	Gajewski 1988	https://doi.org/10.1016/0033-5894(88)90034-8
Deep Lake	Lake sediment	Pollen	P-assemblage	Precip		41.56	-70.64	Marsicek et al., 2013	https://doi.org/10.1016/j.quascirev.2013.09.001
Dixie Lake	Lake sediment	Diatom	D-assemblage	Precip		49.83	-93.95	Laird et al., 2012	https://doi.org/10.1111/j.1365-2486.2012.02740.x
El Malpais	Tree	Tree-rings	Total ring width	Precip		34.97	-108.18	Stahle et al., 2009	https://doi.org/10.1175/2008JCLI2752.1
El Malpais	Tree	Tree-rings	Total ring width	Precip		34.97	-106.18	Grissino and Henri 1995	https://repository.arizona.edu/handle/10150/191192
ELA Lake 239	Lake sediment	Diatom	D-assemblage	Precip		49.67	-93.73	Laird et al., 2012	https://doi.org/10.1111/j.1365-2486.2012.02740.x
ELA Lake 442	Lake sediment	Diatom	D-assemblage	Precip		49.77	-93.82	Laird et al., 2012	https://doi.org/10.1111/j.1365-2486.2012.02740.x
Emerald Lake	Lake sediment	Sediment	GPR	Precip		39.15	-106.41	Shuman et al., 2014	https://doi.org/10.2113/gsrocky.49.1.33
Étang_Fer-de-Lance	Lake sediment	Pollen	P-assemblage	Precip	±80	45.36	-72.23	Claire et al., 2021	https://doi.org/10.1177/0959683621994642
Foy Lake	Lake sediment	Sediment	$\delta^{18}O$	Precip	±35	48.17	-114.35	Spruce et al., 2020	https://doi.org/10.1016/j.qsa.2020.100013
Fresh Pond	Lake sediment	Pollen	P-assemblage	Precip		41.16	-71.58	Jeremiah et al., 2013	https://doi.org/10.1016/j.quascirev.2013.09.001
Gall Lake	Lake sediment	Diatom	D-assemblage	Precip		50.23	-91.45	Kathleen et al., 2011	https://doi.org/10.1111/j.1365-2486.2012.02740.x
Great Basin	Tree	Tree-rings	Total ring width	Temp		38	-116.5	Salzer et al., 2013	https://doi.org/10.1007/s00382-013-1911-9
Greenland-GISP2	Ice core	Ice	d15N & d40Ar	Temp		72.6	-38.5	Kobashi et al., 2010	https://doi.org/10.1007/s10584-009-9689-9
Hell's Kitchen Lake	Lake sediment	Pollen	P-assemblage	Temp, Precip		46.11	-89.42	Gajewski 1988	https://doi.org/10.1016/0033-5894(88)90034-8
Horseshoe Lake (HORM12)	Lake sediment	Sediment	brGDGTs	Temp		38.7	-90.08	Munoz et al., 2020	https://doi.org/10.1029/2020GL087237
Iceberg Lake	Lake sediment	Sediment	Varve thickness	Temp		60.78	-142.95	Loso 2008	https://doi.org/10.1007/s10933-008-9264-9
Jellybean Lake	Lake sediment	Sediment	$\delta^{18}O$	Precip	±5	60.35	-134.8	Anderson et al., 2005	https://doi.org/10.1016/j.yqres.2005.03.005
Juxtlahuaca Cave	Stalagmite	Stalagmite	$\delta^{18}O$	Precip		17.4	-99.2	Lachniet et al., 2017	https://doi.org/10.1130/G32471.1
Kurupa Lake	Lake sediment	Sediment	Chlorophyll	Temp		68.35	-154.61	Boldt et al., 2015	https://doi.org/10.1177/0959683614565929
L1_CANA458	Tree	Tree-rings	Total ring width	Temp		54.21	-71.35	Bellen et al., 2019	https://doi.org/10.1594/PANGAEA.905453
Lake Braya Sø	Lake sediment	Sediment	$U^{k'}37$	Temp		69.99	-51.03	Gunten et al., 2012	https://doi.org/10.1038/srep00609
Lake Mina	Lake sediment	Pollen	P-assemblage	Precip		45.89	-95.48	Jeannine et al., 2020	https://doi.org/10.1016/j.quascirev.2008.01.005
Lake of the Clouds	Lake sediment	Pollen	P-assemblage	Temp, Precip		48	-91.07	Gajewski 1988	https://doi.org/10.1016/0033-5894(88)90034-8
Lake of the Woods	Lake sediment	Sediment	GPR	Precip		43.48	-109.89	Pribyl and Shuman 2014	https://doi.org/10.1016/j.yqres.2014.01.012
Lime lake	Lake sediment	Sediment	$\delta^{18}O$	Precip		48.87	-117.34	Steinman et al., 2012	https://doi.org/10.1073/pnas.1201083109
Little Pond	Lake sediment	Pollen	P-assemblage	Precip		42.68	-72.19	Marsicek et al., 2013	https://doi.org/10.1016/j.quascirev.2013.09.001
Little Raleigh	Lake sediment	Diatom	D-assemblage	Precip		49.45	-91.89	Kathleen et al., 2012	https://doi.org/10.1111/j.1365-2486.2012.02740.x
Meekin Lake	Lake sediment	Diatom	D-assemblage	Precip		49.82	-94.77	Laird et al., 2012	https://doi.org/10.1111/j.1365-2486.2012.02740.x
Minden Bog	Peatland sediment	Sediment	Testate amoeba	Precip		43.61	-82.84	Booth and Jackson, 2003	https://doi.org/10.1191/0959683603hl669rp
Moon Lake	Lake sediment	Diatom	D-assemblage	Precip		46.86	-98.16	Laird et al., 1998	https://doi.org/10.1038/384552a0
Mt Logan	Ice core	Ice	$\delta^{18}O$	Precip		60.58	-140.5	Fisher et al., 2008	https://doi.org/10.1177/0959683608092236
Nevada	Tree	Tree-rings	Total ring width	Precip		38	-117	Huges and Graumlich, 2000	https://doi.org/10.1007/978-3-642-61113-1_6
New Long Pond	Lake sediment	Sediment	GPR	Precip	±40	41.85	-70.68	Newby et al., 2009	https://doi.org/10.1016/j.quascirev.2009.02.020
No Bottom Lake	Lake sediment	Sediment	GPR	Precip		41.29	-70.11	Marsicek et al., 2013	https://doi.org/10.1016/j.quascirev.2013.09.001
Oregon Caves	Stalagmite	Stalagmite	$\delta^{18}O$	Precip		42.08	-123.42	Ersek et al., 2012	https://doi.org/10.1038/ncomms2222
Oro Lake	Lake sediment	Diatom	D-assemblage	Precip		49.78	-105.33	Michels et al., 2007	https://doi.org/10.1111/j.1365-2486.2007.01367.x
Park Range	Lake sediment	Pollen	P-assemblage	Precip		40.7	-106.75	Parish et al., 2020	https://doi.org/10.1017/qua.2019.85
Path Lake	Lake sediment	Pollen	P-assemblage	Precip	±30	43.87	-64.93	Neil et al., 2014	https://doi.org/10.1016/j.yqres.2014.01.001
Renner lake	Lake sediment	Sediment	$\delta^{18}O$	Precip		48.78	-118.19	Steinman et al., 2012	https://doi.org/10.1073/pnas.1201083109
Rogers Lake	Lake sediment	Pollen	P-assemblage	Precip		41.21	-72.17	Marsicek et al., 2013	https://doi.org/10.1016/j.quascirev.2013.09.001
Sharkey Lake	Lake sediment	Pollen	P-assemblage	Precip		44.59	-93.41	Shuman et al., 2016	https://doi.org/10.1016/j.quascirev.2016.03.009
Southern Colorado Plateau	Tree	Tree-rings	Total ring width	Temp, Precip		36.56	-110.12	Salzer and Kipfmueller 2005	https://doi.org/10.1007/s10584-005-5922-3
Southern Sierra Nevada	Tree	Tree-rings	Total ring width	Precip		37.03	-119.43	Touchan et al., 2021	https://doi.org/10.1007/s00382-020-05548-0
Spruce Pond	Lake sediment	Pollen	P-assemblage	Temp		41.24	-74.2	Shuman et al., 2016	https://doi.org/10.1016/j.quascirev.2016.03.009
Steel Lake	Lake sediment	Pollen	P-assemblage	Temp		46.97	-94.68	Shuman et al., 2016	https://doi.org/10.1016/j.quascirev.2016.03.009
White Mountains	Tree	Tree-rings	Total ring width	Temp		37.45	-118.17	Bale et al., 2011	https://doi.org/10.1016/j.yqres.2011.05.004
Baker lake	Tree	Tree-rings	Total ring width	Temp		45.9	-114.3	Hughes et al., 2005	https://doi.org/10.25921/fjr2-x671
Boreal Plateau	Tree	Tree-rings	Total ring width	Temp		36.3	-118.3	Graumlich et al., 2005	https://doi.org/10.25921/6asd-pd54
Cirque Peak	Tree	Tree-rings	Total ring width	Temp		36.3	-118.2	Graybill 1995	https://doi.org/10.25921/vzv9-nc75

Climate
of the Past
Discussions

Table A3. Source and distribution information for precipitation (Precip) and temperature (Temp) across the North American region. (Part-2)

Region	Material	Fractions	Proxy	Variable	Age uncertainty (years)	Latitude	Longitude	Investigators	Publication
Flint Creek Range	Tree	Tree-rings	Total ring width	Temp		46.3	-113.2	Hughes et al., 2005	https://doi.org/10.25921/w5qw-an30
Flower Lake	Tree	Tree-rings	Total ring width	Temp		36.5	-118.2	Graybill 1995	https://doi.org/10.25921/n5aj-jg56
French Glacier	Tree	Tree-rings	Total ring width	Temp		50.8	-115.3	Colenutt et al., 1995	https://doi.org/10.25921/h234-mz90
Kobuk_Noatak	Tree	Tree-rings	Total ring width	Temp		67.1	-159.6	King and Graumlich, 2003	https://doi.org/10.25921/3a2b-f314
Landslide	Tree	Tree-rings	Total ring width	Temp		60.2	-138.5	Luckman et al., 2006	https://doi.org/10.25921/jj5b-h521
Mount Washington	Tree	Tree-rings	Total ring width	Temp		38.5	-114.2	Graybill, 1994	https://doi.org/10.25921/hy54-1r84
Pearl Peak	Tree	Tree-rings	Total ring width	Temp		40.2	-115.5	Graybill, 1994	https://doi.org/10.25921/hy6m-b053
Pintlers	Tree	Tree-rings	Total ring width	Temp		46	-113.4	Gregory et al., 2011	https://doi.org/10.1126/science.1201570
Prince William Sound	Tree	Tree-rings	Total ring width	Temp		60.5	-148.3	Barclay et al., 1999	https://doi.org/10.1191/095968399672825976
San Franciso Peaks	Tree	Tree-rings	Total ring width	Temp		35.3	-111.4	Salzer and Kipfmueller, 2005	https://doi.org/10.1007/s10584-005-5922-3
Sheep Mountain	Tree	Tree-rings	Total ring width	Temp		37.2	-118.1	Graybill 1995	https://doi.org/10.25921/q0we-8b37
Siberian Outpost View	Tree	Tree-rings	Total ring width	Temp		36.5	-118.3	Kipfmueller et al., 2010	https://doi.org/10.1139/X09-187
Spillway Lake	Tree	Tree-rings	Total ring width	Temp		37.8	-119.2	King et al., 2000	https://doi.org/10.25921/v5y4-2w90
Timber Gap Upper	Tree	Tree-rings	Total ring width	Temp		36.3	-118.4	Graybill 1995	https://doi.org/10.25921/vzyy-js91
Upper Wright Lakes	Tree	Tree-rings	Total ring width	Temp		36.4	-118.2	Bunn et al., 2005	https://doi.org/10.1191/0959683605hl827rp
Yellow Mountain Ridge	Tree	Tree-rings	Total ring width	Temp		45.3	-111.3	King et al., 2000	https://doi.org/10.25921/vt0z-ah64
Lac Noir	Lake sediment	Pollen	P-assemblage	Temp		45.8	-75.1	Paquette and Gajewski, 2013	https://doi.org/10.1016/j.quascirev.2013.06.007
Basin pond	Lake sediment	Pollen	P-assemblage	Temp, Precip		44.28	-70.03	Gajewski 1988	https://doi.org/10.1016/0033-5894(88)90034-8

Table A4. Source and distribution information for AMOC, SST, and ITCZ sensitive tracers.

Region	Location	Material	Fractions	Proxy	Variable	Age uncertainty (years)	Latitude	Longitude	Investigators	Publication
Asia	Klang Cave	Stalagmite	Stalagmite	$\delta^{18}O$	ITCZ		8.33	98.73	Tan et al., 2019	https://doi.org/10.1073/pnas.1903167116
Asia	Anjohibe Cave	Stalagmite	Stalagmite	$\delta^{18}O$	ITCZ		-15.53	46.88	Scroxton et al., 2017	https://doi.org/10.1016/j.quascirev.2017.03.017
Asia	Clearwater Cave	Stalagmite	Stalagmite	$\delta^{18}O$	ITCZ		4.1	114.8333	Carolin et al. 2016	https://doi.org/10.1126/science.1233797
Asia	Dongge Cave	Stalagmite	Stalagmite	$\delta^{18}O$	ITCZ		25.283333	108.083333	Wang et al., 2006	https://doi.org/10.1126/science.1106296
Asia	Heshang Cave	Stalagmite	Stalagmite	$\delta^{18}O$	ITCZ		30.45	110.416667	Hu et al., 2008	https://doi.org/10.1016/j.epsl.2007.10.015
Asia	Liang cave	Stalagmite	Stalagmite	$\delta^{18}O$	ITCZ		-8.533333	120.433333	Scroxton et al., 2022	https://doi.org/10.1038/s41598-022-21843-8
Asia	Shenqi Cave	Stalagmite	Stalagmite	$\delta^{18}O$	ITCZ		28.93	103.1	Tan et al., 2018	https://doi.org/10.1016/j.quascirev.2018.07.021
Asia	Tzabnah	Stalagmite	Stalagmite	$\delta^{18}O$	ITCZ		20.733333	-89.466667	Elizalde et al., 2010	https://doi.org/10.1016/j.epsl.2010.08.016
Asia	Wanxiang Cave	Stalagmite	Stalagmite	$\delta^{18}O$	ITCZ		33.316667	105	Zhang et al., 2009	https://doi.org/10.1126/science.1163965
Asia	Yok Balum Cave	Stalagmite	Stalagmite	$\delta^{18}O$	ITCZ		16.2086	-89.0735	Kennett et al., 2012	https://doi.org/10.1126/science.1226299
Asia	Klang Cave	Stalagmite	Stalagmite	$\delta^{18}O$	ITCZ		8.33	98.73	Chawchai et al., 2021	https://doi.org/10.1016/j.quascirev.2020.106779
Asia	Hoti Cave	Stalagmite	Stalagmite	$\delta^{18}O$	ITCZ		23.05	57.21	Fleitmann et al., 2022	https://doi.org/10.1126/science.abg4044
Asia	Botuvera Cave	Stalagmite	Stalagmite	$\delta^{18}O$	ITCZ		-27.223333	-49.155556	Bernal et al., 2016	https://doi.org/10.1016/j.epsl.2016.06.008
Asia	Botuvera Cave	Stalagmite	Stalagmite	$\delta^{18}O$	ITCZ		-29.2233	-49.12	Cruz et al., 2005	https://doi.org/10.1038/nature03365
Australia	Cave KNI-51	Stalagmite	Stalagmite	$\delta^{18}O$	ITCZ		-15.18	128.37	Denniston et al., 2016	https://doi.org/10.1038/srep34485
North America	Juxtlahuaca Cave	Stalagmite	Stalagmite	$\delta^{18}O$	ITCZ		17.4	-99.2	Lachniet et al., 2012	https://doi.org/10.1130/G32471.1
North America	Juxtlahuaca Cave	Stalagmite	Stalagmite	$\delta^{18}O$	ITCZ		17.4	-99.2	Lachniet et al., 2013	https://doi.org/10.1073/pnas.1222804110
North America	Juxtlahuaca Cave	Stalagmite	Stalagmite	$\delta^{18}O$	ITCZ		17.44	-99.16	Lachniet et al., 2017	https://doi.org/10.1016/j.quascirev.2016.11.012
Ocean	KNR166-2 11MC-D	Marine sediment	Sediment	Cd/Ca	AMOC		24.219667	-83.295833	Valley et al., 2022	https://doi.org/10.1029/2021PA004379
Ocean	MD03-2661	Marine sediment	Foraminiferal	$\delta^{13}C$	AMOC	±40	38.89	-76.4	Cronin et al., 2010	https://doi.org/10.1016/j.palaeo.2010.08.009
Ocean	Island of Grimsey	Marine sediment	Molusc	$\delta^{13}C$	AMOC	±30-50	66.53	-18.2	Wanamaker et al., 2012	https://doi.org/10.1038/ncomms1901
Ocean	KN140-2-51	Marine sediment	Sediment	Sortable silt	AMOC	±41.20	32.78	-76.283	Hoffmann et al., 2018	https://doi.org/10.1029/2018GL080187
Ocean	NEAP-4K	Marine sediment	Sediment	Sortable silt	AMOC		61.4985	-24.172167	Thornalley et al., 2013	https://doi.org/10.5194/cp-9-2073-2013
Ocean	ODP983	Marine sediment	Sediment	Sortable silt	AMOC		62.4035	-23.640667	Thornalley et al., 2013	https://doi.org/10.5194/cp-9-2073-2013
Ocean	Orphan Knoll	Marine sediment	Sediment	Sortable silt	AMOC		50.208	-45.688	Hoogakker et al., 2011	https://doi.org/10.1029/2011PA002155
Ocean	MD992251	Marine sediment	Sediment	Sortable silt	AMOC		57.458	-27.913	Hoogakker et al., 2011	https://doi.org/10.1029/2011PA002155
Ocean	GS06-144 08GC	Marine sediment	Sediment	Sortable silt	AMOC		60.3197	-23.966667	Mjell et al., 2014	https://doi.org/10.1002/2014PA002737
Ocean	RAPiD-12-1K	Marine sediment	Foraminiferal	Mg/Ca	SST	±32	62.09	-17.82	Thornalley et al., 2009	https://doi.org/10.1038/nature07717
Ocean	RAPiD-17-5P	Marine sediment	Sediment	Mg/Ca	SST		61.48	-19.54	Sanchez et al., 2014	https://doi.org/10.1038/ngeo2094
Ocean	RAPiD-35-25B	Marine sediment	Foraminiferal	Mg/Ca	SST		38.8863	-76.3947	Sanchez et al., 2014	https://doi.org/10.1002/2013PA002523
Ocean	RD-2209	Marine sediment	Foraminiferal	Mg/Ca	SST		38.89	-76.4	Cronin et al., 2010	https://doi.org/10.1016/j.palaeo.2010.08.009
Ocean	KNR140-2-59GGC	Marine sediment	Foraminiferal	Mg/Ca	SST		32.976995	-76.316001	Arbuszewski et al., 2010	https://doi.org/10.1016/j.epsl.2010.10.035
Ocean	ENAM9606	Marine sediment	Foraminiferal	Mg/Ca	SST		55.650334	-13.985	Richter et al., 2009	https://doi.org/10.1016/j.quascirev.2009.04.008
Ocean	Norwegian Sea	Marine sediment	Alkenone	$U^{k'}37$	SST		60.866129	3.732566	Eiriksson et al., 2006	https://doi.org/10.1177/0959683606hl991rp
Ocean	JR51-GC35	Marine sediment	Sediment	$U^{k'}37$	SST		67.59	-17.56	Bendle & Rosell-Melé, 2007	https://doi.org/10.1177/0959683607073269
Ocean	MD99-2266	Marine sediment	Foraminiferal	$U^{k'}37$	SST	±165	66.23	-24	Moossen et al., 2015	https://doi.org/10.1016/j.quascirev.2015.10.013

470

Competing interests. The authors declare that they have no competing interest.

475

References

Aguiar, W., Meissner, K. J., Montenegro, A., Prado, L., Wainer, I., Carlson, A. E., and Mata, M. M.: Magnitude of the 8.2 ka event freshwater
480   forcing based on stable isotope modelling and comparison to future Greenland melting, Scientific reports, 11, 1–10, 2021.

Allen, J. R., Brandt, U., Brauer, A., Hubberten, H.-W., Huntley, B., Keller, J., Kraml, M., Mackensen, A., Mingram, J., Negendank, J. F.,
        et al.: Rapid environmental changes in southern Europe during the last glacial period, Nature, 400, 740–743, 1999.

Bakker, P., Schmittner, A., Lenaerts, J., Abe-Ouchi, A., Bi, D., van den Broeke, M., Chan, W.-L., Hu, A., Beadling, R., Marsland, S., et al.:
        Fate of the Atlantic Meridional Overturning Circulation: Strong decline under continued warming and Greenland melting, Geophysical
485   Research Letters, 43, 12–252, 2016.

Bell, D. B., Jung, S. J., Kroon, D., Lourens, L. J., and Hodell, D. A.: Local and regional trends in Plio-Pleistocene $\delta18O$ records from benthic
        foraminifera, Geochemistry, Geophysics, Geosystems, 15, 3304–3321, 2014.

Bellomo, K., Angeloni, M., Corti, S., and von Hardenberg, J.: Future climate change shaped by inter-model differences in Atlantic meridional
        overturning circulation response, Nature Communications, 12, 1–10, 2021.

490   Bendle, J. and Rosell-Melé, A.: Distributions of UK37 and UK37′ in the surface waters and sediments of the Nordic Seas: Implications for
        paleoceanography, Geochemistry, Geophysics, Geosystems, 5, 2004.

Bindoff, N. L., Stott, P. A., AchutaRao, K. M., Allen, M. R., Gillett, N., Gutzler, D., Hansingo, K., Hegerl, G., Hu, Y., Jain, S., et al.: Detection
        and attribution of climate change: from global to regional, Climate change 2013: the physical science basis, 2013.

Boers, N.: Observation-based early-warning signals for a collapse of the Atlantic Meridional Overturning Circulation, Nature Climate
495   Change, 11, 680–688, 2021.

Bond, G., Kromer, B., Beer, J., Muscheler, R., Evans, M. N., Showers, W., Hoffmann, S., Lotti-Bond, R., Hajdas, I., and Bonani, G.: Persistent
        solar influence on North Atlantic climate during the Holocene, Science, 294, 2130–2136, 2001.

Böning, C. W., Behrens, E., Biastoch, A., Getzlaff, K., and Bamber, J. L.: Emerging impact of Greenland meltwater on deepwater formation
        in the North Atlantic Ocean, Nature Geoscience, 9, 523–527, 2016.

500   Brovkin, V., Brook, E., Williams, J. W., Bathiany, S., Lenton, T. M., Barton, M., DeConto, R. M., Donges, J. F., Ganopolski, A., McManus,
        J., et al.: Past abrupt changes, tipping points and cascading impacts in the Earth system, Nature Geoscience, pp. 1–9, 2021.

Caesar, L., Rahmstorf, S., Robinson, A., Feulner, G., and Saba, V.: Observed fingerprint of a weakening Atlantic Ocean overturning circula-
        tion, Nature, 556, 191–196, 2018.

Carrillo, C. M., Coats, S., Newman, M., Herrera, D. A., Li, X., Moore, R., Shin, S.-I., Stevenson, S., Lehner, F., and Ault, T. R.: Megadrought:
505   a series of unfortunate La Niña events?, Journal of Geophysical Research: Atmospheres, 127, e2021JD036 376, 2022.

Chawchai, S., Tan, L., Löwemark, L., Wang, H.-C., Yu, T.-L., Chung, Y.-C., Mii, H.-S., Liu, G., Blaauw, M., Gong, S.-Y., et al.: Hydroclimate
        variability of central Indo-Pacific region during the Holocene, Quaternary Science Reviews, 253, 106 779, 2021.

Chen, D., Zhang, P., Seftigen, K., Ou, T., Giese, M., and Barthel, R.: Hydroclimate changes over Sweden in the twentieth and twenty-first
        centuries: a millennium perspective, Geografiska Annaler: Series A, Physical Geography, 103, 103–131, 2021.

510   Chen, G., Norris, J., Neelin, J. D., Lu, J., Leung, L. R., and Sakaguchi, K.: Thermodynamic and dynamic mechanisms for hydrological cycle
        intensification over the full probability distribution of precipitation events, Journal of the Atmospheric Sciences, 76, 497–516, 2019.

Cini, M., Zappa, G., Ragone, F., and Corti, S.: Simulating AMOC tipping driven by internal climate variability with a rare event algorithm,
        npj Climate and Atmospheric Science, 7, 31, 2024.

Clark, P. U., Shakun, J. D., Baker, P. A., Bartlein, P. J., Brewer, S., Brook, E., Carlson, A. E., Cheng, H., Kaufman, D. S., Liu, Z., et al.:
515   Global climate evolution during the last deglaciation, Proceedings of the National Academy of Sciences, 109, E1134–E1142, 2012.

Collins, W. D., Bitz, C. M., Blackmon, M. L., Bonan, G. B., Bretherton, C. S., Carton, J. A., Chang, P., Doney, S. C., Hack, J. J., Henderson,
    T. B., et al.: The community climate system model version 3 (CCSM3), Journal of Climate, 19, 2122–2143, 2006.

Cook, B. I., Smerdon, J. E., Seager, R., and Cook, E. R.: Pan-continental droughts in North America over the last millennium, Journal of
    Climate, 27, 383–397, 2014.

520 Cook, B. I., Smerdon, J. E., Cook, E. R., Williams, A. P., Anchukaitis, K. J., Mankin, J. S., Allen, K., Andreu-Hayles, L., Ault, T. R.,
    Belmecheri, S., et al.: Megadroughts in the Common Era and the Anthropocene, Nature Reviews Earth & Environment, 3, 741–757, 2022.

Couchoud, I., Genty, D., Hoffmann, D., Drysdale, R., and Blamart, D.: Millennial-scale climate variability during the Last Interglacial
    recorded in a speleothem from south-western France, Quaternary Science Reviews, 28, 3263–3274, 2009.

Czaja, A. and Frankignoul, C.: Observed impact of Atlantic SST anomalies on the North Atlantic Oscillation, Journal of Climate, 15, 606–
525   623, 2002.

Dai, A.: Increasing drought under global warming in observations and models, Nature climate change, 3, 52–58, 2013.

Delworth, T. L. and Greatbatch, R. J.: Multidecadal thermohaline circulation variability driven by atmospheric surface flux forcing, Journal
    of Climate, 13, 1481–1495, 2000.

Dima, M., Nichita, D. R., Lohmann, G., Ionita, M., and Voiculescu, M.: Early-onset of Atlantic Meridional Overturning Circulation weak-
530   ening in response to atmospheric CO2 concentration, npj Climate and Atmospheric Science, 4, 27, 2021.

Douville, H., Raghavan, K., Renwick, J., Allan, R. P., Arias, P. A., Barlow, M., Cerezo-Mota, R., Cherchi, A., Gan, T. Y., Gergis, J., et al.:
    Water cycle changes, Sixth Assessment Report of the Intergovernmental Panel on Climate Change, 2021.

Ellison, C. R., Chapman, M. R., and Hall, I. R.: Surface and deep ocean interactions during the cold climate event 8200 years ago, Science,
    312, 1929–1932, 2006.

535 Fordham, D. A., Saltré, F., Haythorne, S., Wigley, T. M., Otto-Bliesner, B. L., Chan, K. C., and Brook, B. W.: PaleoView: a tool for generating
    continuous climate projections spanning the last 21 000 years at regional and global scales, Ecography, 40, 1348–1358, 2017.

Frankignoul, C. and Kestenare, E.: Observed Atlantic SST anomaly impact on the NAO: An update, Journal of climate, 18, 4089–4094,
    2005.

Giannini, A., Kushnir, Y., and Cane, M. A.: Interannual variability of Caribbean rainfall, ENSO, and the Atlantic Ocean, Journal of Climate,
540   13, 297–311, 2000.

Gibson, D. K., Obrist-Farner, J., Birkett, B. A., Curtis, J. H., Berke, M. A., Douglas, P. M., Rice, P. M., and Maurer, J.: The influence of
    tropical Atlantic sea-surface temperatures and the North Atlantic Subtropical High during the Maya Droughts, The Holocene, 34, 212–223,
    2024.

Gonzalez-Rouco, J., Fernández-Donado, L., Raible, C., Barriopedro, D., Lutherbacher, J., Jungclaus, J., Swingedouw, D., Servonnat, J.,
545   Zorita, E., Wagner, S., et al.: Medieval Climate Anomaly to Little Ice Age transition as simulated by current climate models, PAGES
    news, 19, 7–8, 2011.

Graham, N. E., Ammann, C., Fleitmann, D., Cobb, K., and Luterbacher, J.: Support for global climate reorganization during the "Medieval
    Climate Anomaly", Climate dynamics, 37, 1217–1245, 2011.

Gupta, A. K., Anderson, D. M., and Overpeck, J. T.: Abrupt changes in the Asian southwest monsoon during the Holocene and their links to
550   the North Atlantic Ocean, Nature, 421, 354–357, 2003.

Climate
of the Past
Discussions

Helama, S., Meriläinen, J., and Tuomenvirta, H.: Multicentennial megadrought in northern Europe coincided with a global El Niño–Southern Oscillation drought pattern during the Medieval Climate Anomaly, Geology, 37, 175–178, 2009.

Held, I. M. and Soden, B. J.: Robust responses of the hydrological cycle to global warming, Journal of climate, 19, 5686–5699, 2006.

Hernández, A., Sánchez-López, G., Pla-Rabes, S., Comas-Bru, L., Parnell, A., Cahill, N., Geyer, A., Trigo, R. M., and Giralt, S.: A 2,000-year
555   Bayesian NAO reconstruction from the Iberian Peninsula, Scientific reports, 10, 1–15, 2020.

Hobeichi, S., Abramowitz, G., Ukkola, A. M., De Kauwe, M., Pitman, A., Evans, J. P., and Beck, H.: Reconciling historical changes in the hydrological cycle over land, npj Climate and Atmospheric Science, 5, 1–9, 2022.

Hoffmann, S. S., Dalsing, R. E., and Murphy, S. C.: Sortable silt records of intermediate-depth circulation and sedimentation in the Southwest Labrador Sea since the Last Glacial Maximum, Quaternary Science Reviews, 206, 99–110, 2019.

560   Holliday, N. P., Bersch, M., Berx, B., Chafik, L., Cunningham, S., Florindo-López, C., Hátún, H., Johns, W., Josey, S. A., Larsen, K. M. H.,
et al.: Ocean circulation causes the largest freshening event for 120 years in eastern subpolar North Atlantic, Nature communications, 11,
1–15, 2020.

Hong, Y., Wang, Z., Jiang, H., Lin, Q., Hong, B., Zhu, Y., Wang, Y., Xu, L., Leng, X., and Li, H.: A 6000-year record of changes in drought and precipitation in northeastern China based on a $\delta13C$ time series from peat cellulose, Earth and Planetary Science Letters, 185,
565   111–119, 2001.

Huang, J., Yu, H., Guan, X., Wang, G., and Guo, R.: Accelerated dryland expansion under climate change, Nature climate change, 6, 166–171,
2016.

Hurrell, J. W. and Deser, C.: North Atlantic climate variability: the role of the North Atlantic Oscillation, Journal of marine systems, 79,
231–244, 2010.

570   Jackson, L., Kahana, R., Graham, T., Ringer, M., Woollings, T., Mecking, J., and Wood, R.: Global and European climate impacts of a slowdown of the AMOC in a high resolution GCM, Climate dynamics, 45, 3299–3316, 2015.

Jones, E. P. and Anderson, L. G.: Is the global conveyor belt threatened by Arctic Ocean fresh water outflow?, in: Arctic–Subarctic Ocean Fluxes, pp. 385–404, Springer, 2008.

Kilbourne, K. H., Wanamaker, A. D., Moffa-Sanchez, P., Reynolds, D. J., Amrhein, D. E., Butler, P. G., Gebbie, G., Goes, M., Jansen, M. F.,
575   Little, C. M., et al.: Atlantic circulation change still uncertain, Nature Geoscience, 15, 165–167, 2022.

Kim, H.-J., An, S.-I., Park, J.-H., Sung, M.-K., Kim, D., Choi, Y., and Kim, J.-S.: North Atlantic Oscillation impact on the Atlantic Meridional Overturning Circulation shaped by the mean state, npj Climate and Atmospheric Science, 6, 25, 2023.

Konecky, B. L., McKay, N. P., Falster, G. M., Stevenson, S. L., Fischer, M. J., Atwood, A. R., Thompson, D. M., Jones, M. D., Tyler, J. J.,
DeLong, K. L., et al.: Globally coherent water cycle response to temperature change during the past two millennia, Nature Geoscience,
580   pp. 1–8, 2023.

Kriegler, E., Hall, J. W., Held, H., Dawson, R., and Schellnhuber, H. J.: Imprecise probability assessment of tipping points in the climate system, Proceedings of the national Academy of Sciences, 106, 5041–5046, 2009.

Kuhlbrodt, T., Griesel, A., Montoya, M., Levermann, A., Hofmann, M., and Rahmstorf, S.: On the driving processes of the Atlantic meridional overturning circulation, Reviews of Geophysics, 45, 2007.

585   LaMarche Jr, V. C.: Paleoclimatic Inferences from Long Tree-Ring Records: Intersite comparison shows climatic anomalies that may be linked to features of the general circulation., Science, 183, 1043–1048, 1974.

Lamb, H. H.: Climatic fluctuations, World survey of climatology, 2, 173–249, 1969.

Latif, M., Sun, J., Visbeck, M., and Hadi Bordbar, M.: Natural variability has dominated Atlantic Meridional Overturning Circulation since 1900, Nature Climate Change, 12, 455–460, 2022.

590 Lehner, F., Born, A., Raible, C. C., and Stocker, T. F.: Amplified inception of European Little Ice Age by sea ice–ocean–atmosphere feedbacks, Journal of climate, 26, 7586–7602, 2013.

Levy, E. J., Vonhof, H. B., Bar-Matthews, M., Martínez-García, A., Ayalon, A., Matthews, A., Silverman, V., Raveh-Rubin, S., Zilberman, T., Yasur, G., et al.: Weakened AMOC related to cooling and atmospheric circulation shifts in the last interglacial Eastern Mediterranean, Nature communications, 14, 5180, 2023.

595 Liu, W., Fedorov, A. V., Xie, S.-P., and Hu, S.: Climate impacts of a weakened Atlantic Meridional Overturning Circulation in a warming climate, Science advances, 6, eaaz4876, 2020.

Lynch-Stieglitz, J.: The Atlantic meridional overturning circulation and abrupt climate change, Annual review of marine science, 9, 83–104, 2017.

Mann, M. E., Zhang, Z., Rutherford, S., Bradley, R. S., Hughes, M. K., Shindell, D., Ammann, C., Faluvegi, G., and Ni, F.: Global signatures

600 and dynamical origins of the Little Ice Age and Medieval Climate Anomaly, Science, 326, 1256–1260, 2009.

Marchitto Jr, T. M., Oppo, D. W., and Curry, W. B.: Paired benthic foraminiferal Cd/Ca and Zn/Ca evidence for a greatly increased presence of Southern Ocean Water in the glacial North Atlantic, Paleoceanography, 17, 10–1, 2002.

Marshall, J., Donohoe, A., Ferreira, D., and McGee, D.: The ocean's role in setting the mean position of the Inter-Tropical Convergence Zone, Climate Dynamics, 42, 1967–1979, 2014.

605 Masson-Delmotte, V., Zhai, P., Pirani, A., Connors, S. L., Péan, C., Berger, S., Caud, N., Chen, Y., Goldfarb, L., Gomis, M., et al.: Climate change 2021: the physical science basis, Contribution of working group I to the sixth assessment report of the intergovernmental panel on climate change, 2, 2021.

McCarthy, G. D., Smeed, D. A., Johns, W. E., Frajka-Williams, E., Moat, B. I., Rayner, D., Baringer, M. O., Meinen, C. S., Collins, J., and Bryden, H. L.: Measuring the Atlantic meridional overturning circulation at 26 N, Progress in Oceanography, 130, 91–111, 2015.

610 Moffa-Sánchez, P., Moreno-Chamarro, E., Reynolds, D., Ortega, P., Cunningham, L., Swingedouw, D., Amrhein, D. E., Halfar, J., Jonkers, L., Jungclaus, J. H., et al.: Variability in the northern North Atlantic and Arctic oceans across the last two millennia: A review, Paleoceanography and Paleoclimatology, 34, 1399–1436, 2019.

Oglesby, J., Feng, S., Hu, Q., and Rowe, C.: Medieval drought in North America: The role of the Atlantic multidecadal oscillation, PAGES news, 19, 18–19, 2011.

615 Pratap, S. and Markonis, Y.: The response of the hydrological cycle to temperature changes in recent and distant climatic history, Progress in Earth and Planetary Science, 9, 1–37, 2022.

R Core Team, A., Team, R. C., et al.: R: A language and environment for statistical computing. R Foundation for Statistical Computing, Vienna, Austria. 2012, 2022.

Rahmstorf, S.: Shifting seas in the greenhouse?, Nature, 399, 523–524, 1999.

620 Robson, J., Hodson, D., Hawkins, E., and Sutton, R.: Atlantic overturning in decline?, Nature Geoscience, 7, 2–3, 2014.

Santos, T. P., Ballalai, J. M., Franco, D. R., Oliveira, R. R., Lessa, D. O., Venancio, I. M., Chiessi, C. M., Kuhnert, H., Johnstone, H., and Albuquerque, A. L. S.: Asymmetric response of the subtropical western South Atlantic thermocline to the Dansgaard-Oeschger events of Marine Isotope Stages 5 and 3, Quaternary Science Reviews, 237, 106 307, 2020.

Schmidt, M. W., Spero, H. J., and Lea, D. W.: Links between salinity variation in the Caribbean and North Atlantic thermohaline circulation,

625 Nature, 428, 160–163, 2004.

Seager, R., Graham, N., Herweijer, C., Gordon, A. L., Kushnir, Y., and Cook, E.: Blueprints for Medieval hydroclimate, Quaternary Science Reviews, 26, 2322–2336, 2007.

Seager, R., Burgman, R., Kushnir, Y., Clement, A., Cook, E., Naik, N., and Miller, J.: Tropical Pacific forcing of North American medieval megadroughts: Testing the concept with an atmosphere model forced by coral-reconstructed SSTs, Journal of Climate, 21, 6175–6190, 2008.

Srokosz, M. and Bryden, H.: Observing the Atlantic Meridional Overturning Circulation yields a decade of inevitable surprises, Science, 348, 1255 575, 2015.

Steiger, N. J., Smerdon, J. E., Cook, E. R., and Cook, B. I.: A reconstruction of global hydroclimate and dynamical variables over the Common Era, Scientific data, 5, 1–15, 2018.

Steinman, B. A., Stansell, N. D., Mann, M. E., Cooke, C. A., Abbott, M. B., Vuille, M., Bird, B. W., Lachniet, M. S., and Fernandez, A.: Interhemispheric antiphasing of neotropical precipitation during the past millennium, Proceedings of the National Academy of Sciences, 119, e2120015 119, 2022.

Studholme, J., Fedorov, A. V., Gulev, S. K., Emanuel, K., and Hodges, K.: Poleward expansion of tropical cyclone latitudes in warming climates, Nature Geoscience, 15, 14–28, 2022.

Sutton, R. T. and Hodson, D. L.: Atlantic Ocean forcing of North American and European summer climate, science, 309, 115–118, 2005.

Tabari, H.: Climate change impact on flood and extreme precipitation increases with water availability, Scientific reports, 10, 13 768, 2020.

Tan, L., Shen, C.-C., Löwemark, L., Chawchai, S., Edwards, R. L., Cai, Y., Breitenbach, S. F., Cheng, H., Chou, Y.-C., Duerrast, H., et al.: Rainfall variations in central Indo-Pacific over the past 2,700 y, Proceedings of the national academy of sciences, 116, 17 201–17 206, 2019.

Thackeray, C. W., Hall, A., Norris, J., and Chen, D.: Constraining the increased frequency of global precipitation extremes under warming, Nature Climate Change, 12, 441–448, 2022.

Trenberth, K. E., Dai, A., Rasmussen, R. M., and Parsons, D. B.: The changing character of precipitation, Bulletin of the American Meteorological Society, 84, 1205–1218, 2003.

Trenberth, K. E., Jones, P. D., Ambenje, P., Bojariu, R., Easterling, D., Klein Tank, A., Parker, D., Rahimzadeh, F., Renwick, J. A., Rusticucci, M., et al.: Observations. surface and atmospheric climate change. Chapter 3, Fourth Assessment Report of the Intergovernmental Panel on Climate Change, 2007.

Trouet, V., Esper, J., Graham, N. E., Baker, A., Scourse, J. D., and Frank, D. C.: Persistent positive North Atlantic Oscillation mode dominated the medieval climate anomaly, science, 324, 78–80, 2009.

Trouet, V., Scourse, J., and Raible, C.: North Atlantic storminess and Atlantic Meridional Overturning Circulation during the last Millennium: Reconciling contradictory proxy records of NAO variability, Global and Planetary Change, 84, 48–55, 2012.

Valley, S. G., Lynch-Stieglitz, J., Marchitto, T. M., and Oppo, D. W.: Seawater cadmium in the Florida Straits over the Holocene and implications for upper AMOC variability, Paleoceanography and Paleoclimatology, 37, e2021PA004 379, 2022.

Vellinga, M. and Wood, R. A.: Global climatic impacts of a collapse of the Atlantic thermohaline circulation, Climatic change, 54, 251–267, 2002.

Wanamaker, A. D., Butler, P. G., Scourse, J. D., Heinemeier, J., Eiríksson, J., Knudsen, K. L., and Richardson, C. A.: Surface changes in the North Atlantic meridional overturning circulation during the last millennium, Nature Communications, 3, 1–7, 2012.

Wei, G., Sun, M., Li, X., and Nie, B.: Mg/Ca, Sr/Ca and U/Ca ratios of a porites coral from Sanya Bay, Hainan Island, South China Sea and their relationships to sea surface temperature, Palaeogeography, Palaeoclimatology, Palaeoecology, 162, 59–74, 2000.

Weijer, W., Cheng, W., Drijfhout, S. S., Fedorov, A. V., Hu, A., Jackson, L. C., Liu, W., McDonagh, E., Mecking, J., and Zhang, J.: Stability
665   of the Atlantic Meridional Overturning Circulation: A review and synthesis, Journal of Geophysical Research: Oceans, 124, 5336–5375,
         2019.

Weijer, W., Cheng, W., Garuba, O. A., Hu, A., and Nadiga, B.: CMIP6 models predict significant 21st century decline of the Atlantic
         meridional overturning circulation, Geophysical Research Letters, 47, e2019GL086 075, 2020.

Woollings, T.: Dynamical influences on European climate: An uncertain future, Philosophical Transactions of the Royal Society A: Mathe-
670   matical, Physical and Engineering Sciences, 368, 3733–3756, 2010.

Zhuravleva, A., Bauch, H. A., Mohtadi, M., Fahl, K., and Kienast, M.: Caribbean salinity anomalies contributed to variable North Atlantic
         circulation and climate during the Common Era, Science Advances, 9, eadg2639, 2023.